SBUF

ID: 13686 & 13931

SKANSKA

KTH

PROCESS OCH KVALITETSKONTROLL AV INJEKTERING

John Shamu

December 2021

SBUF stödjer
forskning & utveckling
som leder till
praktisk handling

KTH ROYAL INSTITUTE
OF TECHNOLOGY

Doctoral Thesis in Civil and Architectural Engineering

Rock grouting design: Rheological aspects and radial flow visualizations with ultrasound

TAFADZWA JOHN SHAMU

Stockholm, Sweden 2021

Rock grouting design: Rheological aspects and radial flow visualizations with ultrasound

TAFADZWA JOHN SHAMU

Academic Dissertation which, with due permission of the KTH Royal Institute of Technology, is submitted for public defence for the Degree of Doctor of Philosophy on Thursday the 2nd of December 2021, at 15:00 p.m. in F3, Lindstedsvägen 26, Stockholm.

Doctoral Thesis in Civil and Architectural Engineering
KTH Royal Institute of Technology
Stockholm, Sweden 2021

TRITA-ABE-DLT-2140
ISBN 978-91-8040-029-9

Printed by: Universitetsservice US-AB, Sweden 2021

Abstract

The rheological properties of cement-based grouts play a crucial role in determining the final spread in grouted rock formations. In rheological terms, cement grouts are known to be complex time-dependent yield stress fluids, but their steady flow behavior is often described by the simple Bingham constitutive law. The Bingham parameters obtained from the linear curve fitting to flow curve data are then used in grout propagation calculations during the design phase, e.g., for rock fracture grouting in tunnel construction. Since cement grouts are time-dependent and thixotropic suspensions, the interpretation of their flow curves during conventional rotational rheometry is often complicated by the presence of wall slip, thixotropy, flow localization, and sedimentation, particularly at low shear rates. A systematic approach was carried out as part of the research work to study these effects within the constraints of the concentric cylinder geometry (Couette) and for different cement grout concentrations. Of particular interest were the influence of geometry and flow sweep measurement interval on flow curves, including the characteristic unstable flow branch that appears at applied shear rates that are below the critical shear rate. The unstable flow branch observed below the critical shear rate has been described as a characteristic feature in the flow curves of thixotropic suspensions, e.g., cement grouts and laponite. From a practical standpoint, these crucial shear rate aspects, including wall slip, have not been considered during grouting design calculations while using the common Bingham model. Thus, the research also considered these shear rate aspects as part of grouting design by incorporating them into the design approach within the existing framework of the Real Time Grouting Control (RTGC) method.

Another interesting part of the research work presented in this thesis relates to studies on the radial flow of yield stress fluids. The radial flow between parallel plates is an idealized fundamental flow configuration that is often used to understand grout spread estimation in rock fractures. In part, the entire radial flow work was motivated by the ongoing discussions in the literature regarding the different analytical solutions for radial flow. Moreover, compared to other flow configurations, e.g., pipes and channels, only a limited amount of work has presented analytical solutions, numerical models, and especially experimental work for radial flow. Thus, during the doctoral work, a radial flow experimental device was designed, manufactured, and subsequently used to acquire Carbopol YSF radial flow velocity profiles for the first time. The velocity profile measurements were carried out using the pulsed Ultrasound Velocity Profiling (UVP) technique. The velocity profiles from the initial radial flow study showed that significant wall slip

was present. An analytical solution with a Navier slip term was used to describe the velocity profiles, resulting in a good agreement in the velocity profile magnitude. However, the plug-flow region extent was smaller in the analytical solution. Subsequent studies on radial flow sought to address the wall slip issue using different wall slip reduction procedures (chemical treatment and sandblasting). Both treatments showed substantial wall slip reduction; however, some wall slip effects persisted, especially for the thicker Carbopol gels. In addition, a plug-point estimation algorithm using Tikhonov regularization was developed to calculate the yield points from the non-smooth velocity profiles accurately. A final modification was the addition of frame reinforcement to maintain the required constant aperture better. The tests carried out in the final radial flow study followed the test scheme from the previous studies, but with two concentrations of Carbopol. The aim was to compare the measured velocity profiles with two radial flow analytical solutions based on different assumptions that have recently been discussed in the literature. The measurement results showed a good agreement in the velocity profile shape, but with some velocity magnitude discrepancies, particularly in the central part of the velocity profiles. Such discrepancies could result from remaining wall slip together with other higher-order flow effects, e.g., nonlinear flow due to inertial effects, that are not accounted for by the analytical solutions. Nevertheless, within the context of grouting practice, such magnitudes of differences could be considered reasonable for scoping calculations during grouting design and execution. Future studies related to radial flow can improve the current understanding by conducting similar tests, but with improved experimental setups, e.g., better wall slip reduction, larger aspect ratios, and more detailed spatial resolution for smaller flow apertures. Additionally, the understanding of the rheological behavior of cement grouts would be improved from a practical standpoint, i.e., grouting design and execution, if the wall slip phenomenon is studied in more detail and considered an inseparable feature of yield stress fluid flow.

Keywords: Cement grouts; grouting; yield stress fluid (YSF); thixotropy; critical shear rate; radial flow; wall slip; Bingham model.

Sammanfattning

Cementbaserade injekteringsmedels reologiska egenskaper har en stor påverkan på strömning och inträngningslängd i sprickigt berg. Medlens reologi är komplex, inklusive tixotropi, men strömningen och inträngningen beskrivs ändå oftast med den enkla linjära Bingham modellen i injekteringssammanhang. De två parametrarna från denna modell, flytgräns och viskositet, används sedan inom injekteringsprojektering, för t.ex. tunnlar och dammar, för att bedöma inträngningen. Eftersom cementbaserade medel är tixoptropa suspensioner försvåras utvärderingen vid mätning med konventionella rotationsviskometrar på grund av glidning vid fasta begränsningsytor, sedimentation/separation av partiklarna och instabila flöden vid låga deformationshastigheter. En systematisk mätprocedur för att studera ovanstående problem med rotationsviskometer och koncentriska cylindrar samt olika vanliga vattencementtal, har utförts inom ramen för detta doktorandarbete. Av särskilt intresse har varit att studera effekten av olika geometrier och tidsintervallet mellan mätningarna, inklusive den instabila delen av flödeskurvan då deformationshastigheten är lägre än ett kritiskt värde. Denna del av kurvan har i litteraturen beskrivits som karakteristisk för tixotropa suspensioner, som t.ex. cementbaserade injekteringsmedel. Praktiskt kan ovanstående kunskap användas för att förbättra mätningen av de reologiska egenskaperna. Existensen av en kritisk deformationshastighet under vilken det inte finns något stabilt flöde, i kombination med glidning vid fasta begränsningsytor, diskuteras särskilt med hänsyn till dess påverkan på faktisk inträngning i släta och råa bergsprickor.

Ett annat fokus i doktorandarbetet har varit att studera icke-Newtonska modellvätskors (Carbopol) radiella strömning mellan parallella plattor. Denna typ av strömningsgeometri används ofta som en idealiserad konfiguration för strömning i bergsprickor. I jämförelse med andra enklare geometrier, finns endast en begränsad forskning utförd för denna geometri både då det gäller analytiska och numeriska beräkningar men framförallt då det gäller experiment. Som ett första steg inför en mer systematisk undersökning av icke-Newtonsk radiella strömning presenteras i detta arbete framtagandet av en fysisk laboratoriemodell där hastighetsprofilerna mellan plattorna för första gången visualiserats med hjälp av ultraljud. De utförda mätningarna med tre olika öppningar mellan plattorna sam tre olika värden på det konstanta flödet, visar på en distinkt plugg som är ett resultat av vätskans flytgräns samt glidning i gränsskiktet mellan vätskan och plattornas fasta begränsningsytor. En jämförelse mellan uppmätta hastighetsprofiler och analytiskt beräknade diskuteras där resultaten överensstämmer relativt väl, med beaktande av de långtgående förenklade antaganden som krävs för de

analytiska beräkningarna. Fortsatta studier kommer att fokuseras på att förbättra laboratoriemodellen för en mer detaljerad studie av icke-Newtonska vätskors strömning och hur pluggen utvecklas under den radiella inträngningen, vilket fortsättningsvis är av betydelse för projektering av injektering i bergsprickor.

Nyckelord: Cementbaserade injekteringsmedels; injektering; icke-Newtonska vätskors; tixotropi; kritisk deformationshastigheten; radiella strömning; glidning; Bingham modell.

Preface

This doctoral thesis is a summary of the research work on rock grouting design. The work is primarily experimental, focusing on rheological aspects, including conventional rheometry, ultrasound-based velocimetry, and analytical analyses. Most of the work was carried out at the Division of Soil and Rock Mechanics at the KTH Royal Institute of Technology in Stockholm, Sweden. All cement rheology tests were conducted at KTH. The initial experimental work related to the radial flow tests was carried out at Incipientus AB, Gothenburg. The rest of the radial flow tests (last two papers) were completed at the Concrete laboratory at KTH Byggvetenskap.

The work was supervised by Dr. Ulf Håkansson at Skanska/KTH, Professor Stefan Larsson at KTH, and co-supervised by Dr. Liangchao Zou, also at KTH. Their support, encouragement, and valuable insights are greatly appreciated. More so, Dr. Ulf Håkansson provided a great deal of guidance, especially in the early stages of the doctoral program when I had just arrived and had minimal knowledge of rheology and how it relates to the field of grouting. Additionally, I would like to thank Dr. Johan Wiklund, Dr. Reinhardt Kotzé, and Michal Kotzé at Incipientus AB for their contributions, especially during my occasional stays in Göteborg.

The experience and input from my reference group are also gratefully acknowledged. Many thanks to colleagues and friends at the Division of Soil and Rock Mechanics; their engaging questions during our group seminars were constructive. Not forgetting the discussions with my friend Everett that were particularly helpful towards the end, as we shared our mutual difficulties with the doctoral work. Last but certainly not least, I am grateful towards my mother Beatrice, and my partner Kristin, for their beloved and continued support.

Funding acknowledgement

The research presented in this thesis was funded by the Swedish Construction Industry's Organization for Research and Development (SBUF) and co-funded by the Swedish Rock Engineering Research Foundation (BeFo). Their support is gratefully acknowledged.

List of appended papers

Paper I
T.J. Shamu & U. Håkansson, 2019.
Rheology of cement grouts: On the critical shear rate and no-slip regime in the Couette geometry.
Cement and Concrete Research. Volume 123, 105769.

Paper II
T.J. Shamu, L. Zou, & U. Håkansson, 2021.
A nomogram for cement-based rock grouting design.
Tunneling and Underground Space Technology. 116 (October 2021): 104110.

Paper III
T.J. Shamu, L. Zou, R. Kotzé, J. Wiklund, & U. Håkansson, 2020.
Radial flow velocity profiles of a yield stress fluid between smooth parallel disks.
Rheologica Acta. 59, 239–254.

Paper IV
T.J. Shamu, L. Zou, & U. Håkansson, 2021.
An experimental device for measuring radial flow velocity profiles of yield stress fluids.
Accepted for publication: Flow Measurement and Instrumentation.

Paper V
T.J. Shamu, L. Zou, & U. Håkansson, 2021.
Radial flow of yield stress fluids: an experimental and theoretical study.
Submitted: Journal of Rock Mechanics and Geotechnical Engineering.

Division of work between authors

Ulf Håkansson was responsible for acquiring funds and resources related to the project work, as well as supervising the individual research projects leading up to the final scientific articles.

Paper I: John Shamu carried out the experimental work and wrote the paper. Ulf Håkansson contributed with his comments.

Paper II: John Shamu designed the experimental model and performed the experiments. Liangchao Zou contributed to the analytical solution. Reinhardt Kotzé and Johan Wiklund supervised the experimental work at Incipientus, Göteborg. The paper was written by John Shamu with input from all co-authors.

Paper III: John Shamu wrote the paper with inputs from Liangchao Zou and Ulf Håkansson. John Shamu carried out the experimental work.

Paper IV: John Shamu performed the experiments and wrote the paper with inputs from Liangchao Zou and Ulf Håkansson. Both Ulf Håkansson and Liangchao Zou contributed with comments to the paper.

Paper V: John Shamu carried out the experiments. Liangchao Zou contributed to the theoretical analyses. John Shamu then wrote the paper with inputs from Liangchao Zou and Ulf Håkansson.

Other articles and publications

Articles produced during the doctoral work, but not included in this thesis:

T.J. Shamu, L. Zou, U. Håkansson, 2019. Cementbaserade Injekteringsmedels Reogram: Instabilt Flöde Och Inverkan På Injektering. i Proceedings Bergdagarna, Stockholm.

T.J. Shamu, L. Zou, U. Håkansson,2019. An experimental study of 2D radial flow of a yield stress fluid between parallel disks. In: Nordic Grouting Symposium, Helsinki, Finland, 2019.

T.J. Shamu, 2019. On the measurement and application of cement grout rheological properties (Licentiate Dissertation). KTH Royal Institute of Technology, Stockholm.

S. Zade, T.J. Shamu, F. Lundell, L. Brandt, 2020. Finite-size spherical particles in a square duct flow of an elastoviscoplastic fluid: an experimental study. J. Fluid Mech. 883, A6.

T.J. Shamu, L. Zou, U. Håkansson, 2021. Cement-based rock grouting: shear rate dependencies. Submitted to 6th International Conference on Grouting and Deep Mixing, New Orleans, Louisiana, USA.

Contents

Nomenclature

Acronyms and abbreviations

1D	One dimensional
2D	Two dimensional
ACG	Aperture Controlled Grouting
CUSUM	Cumulative Sum
GIN	Grouting Intensity Number
HB	Herschel-Bulkley
NARC	North American Refusal Criterion
RTGC	Real Time Grouting Control
UVP	Ultrasound Velocity Profiling
w/c	Water to cement ratio
YSF	Yield Stress Fluid

Symbols and constants

ΔP	Effective grouting pressure
$\dot{\gamma}_c$	Critical shear rate
$\dot{\gamma}_{D_{wall}}$	Dimensionless wall shear rate
$\dot{\gamma}_{ns}$	No-slip shear rate
$\dot{\gamma}_{wall}$	Wall shear rate
Γ	Shear rate constant
γ	Steering parameter
μ_B	Plastic viscosity
τ_0	Yield stress
τ_B	Bingham yield stress
I_D	Dimensionless propagation length
I_{max}	Maximum propagation length
k	Consistency coefficient
n	Flow index
Q	Volume flow rate
Q_D	Dimensionless volume flow rate
t_0	Characteristic time
t_D	Dimensionless time

Chapter 1

Introduction

1.1 Background

Cement-based grouting is a construction method that has long been used to seal off water flow in structures such as tunnels, caverns, and dam foundations (Louis, 1969, Håkansson, 1993, Lombardi and Deere, 1993, Gustafson and Stille, 2005, Funehag, 2007, Fransson et al., 2016, Nejad Ghafar, 2017, Rahman et al., 2017, Shamu and Håkansson, 2019, Hoang et al., 2021). In addition, the technique is also used to improve the mechanical properties of weak soil or fractured rock masses (U. S. Army Corps of Engineers, 2017). The grouting industry often prefers cement-based grouts to other chemical-based grouts because of their relatively low cost, combined with the fact that they pose less of a risk as a pollutant, especially to underground water resources.

In rock grouting applications, it is often necessary to estimate the expected grouting efficiency or sealing effect that can be achieved. However, this is not a trivial task, as the overall efficiency of a typical grouting operation is in fact a complex multi-factored process. The main factors that contribute to the efficiency of a grouting operation can be broadly grouped into those attributable to: (i) the rock fracture geometry, (ii) grouting design and execution, and (iii) the flow properties of the cement grouts, i.e., their rheological properties including their penetrability; see (Håkansson, 1993, Banfill and Saunders, 1981, Draganović and Stille, 2014). Briefly, *rheology* is defined as the *science of the deformation and flow of matter*. The term was coined by Eugene C. Bingham, a professor at Lafayette College, in the 1920s. Another definition that is more applicable to this thesis: Rheology is the characterization of materials using 'constitutive equations' that relate the stress history and strain history; see Doraiswamy (2002) and Barnes and Hutton (1989).

A factor such as the rock fracture geometry is more often than not hard to accurately determine through measurement. Moreover, such a factor is not readily presentable as a tunable grouting parameter for grouting

applications when compared to the rheological properties of cement grouts. As such, more research progress has been seen on the development of tools, materials and methods to achieve application specific cement grouts with controllable flow properties (Houlsby, 1990, Håkansson, 1993, Roussel, 2016). Furthermore, previous analytical, numerical and experimental studies that focus on grout rheology have to a greater degree demonstrated how the rheological properties significantly influence grout propagation, and consequently the estimated final spread that can be achieved in grouted rock fractures (Håkansson, 1993, Gustafson et al., 2013, Draganović and Stille, 2014, Nejad Ghafar, 2017). Similarly, this thesis continues with the focused development on improving experimental approaches and analytical tools that would aid researchers and practitioners alike with, e.g., analytical grouting design approaches and practical knowledge on cement grout rheology that can be readily implemented.

A starting point in understanding the key rheological properties of cement grouts is through conventional rotational rheometry under controlled conditions, i.e., by imposing known shear stresses or shear rates on a sample of grout suspension and then measuring the corresponding shear rates or shear stresses as output. To perform such experiments, several test methods for the field and laboratory have been developed, with the most common laboratory test being offline rotational rheometry with coaxial shearing geometry (Couette) Barnes and Hutton (1989), Chhabra and Richardson (2008), Ovarlez (2012). The resultant shear stress-shear rate data from rotational rheometry are often plotted on diagrams commonly referred to as flow curves. Interpretations of the flow curves are normally carried out by using rheological models (constitutive equations). These models relate the shear stress and shear rate to describe the flow behavior of a fluid (e.g., any cement grout) from a macroscopic point of view, i.e., with a given set of parameters. The macroscopic point of view deals with flow on a scale involving overall structures or processes rather than individual microscopic components, which are considered in the microscopic view. Constitutive equations can be derived from a macroscopic and/or microscopic point of view; see Barnes and Hutton (1989).

One example of such a rheological model is the Bingham model, a simplified two parameter model often used to describe the flow behavior of cementitious suspensions that possess a yield stress component. The Bingham model together with others, e.g., the Herschel-Bulkley (HB) model and Casson model are usually used to describe the yield stress rheological behavior of cements and other mineral suspensions (Van Wazer et al., 1963, Kelessidis et al., 2006). The defining feature of these Yield Stress Fluids

(YSFs) is a yield (critical) stress value τ_0 that needs to be exceeded by the driving force or shear stress in order to initiate flow. Unlike common fluids such as pure water and less viscous oils that flow immediately after being poured, YSFs are structured fluids (i.e., composed of stronger structural links or physical interactions between constituent elements) that need to be first broken down in order to initiate flow (Balmforth et al., 2014, Frigaard, 2019). The outlined rheological models offer at least some way to capture this important yield stress, which has been a topic of extensive discussion within the literature.(Moller et al., 2009, Barnes, 2007)

Despite the utility of such rheological models in simplifying grouting design calculations, they often do not encompass some key shear rate aspects of cement grouts such as wall slip and various forms of flow localization. Wall slip of particle suspensions has been discussed within the literature, however its impacts on the grouting process have never been assessed; the same can be said for the different types of flow localization.

Within the rheological literature on suspensions similar to cements etc., specific forms of flow localization have been described as: (i) shear localization, a form of localization induced by the geometry, i.e., shear rate variations due to the shape of the shear geometry result in static fluid bands beyond some spatial distance where the shear rate is below a critical value, and (ii) shear banding, a common flow phenomena in thixotropic suspensions, wherein for the same applied shear rate flowing and static bands of material coexist; shear banding occurs below a material dependent critical shear rate $\dot{\gamma}_c$ (Divoux et al., 2016). The latter form of localization has been shown as a widespread intrinsic characteristic of thixotropic suspensions e.g., cement grouts, laponite and drilling mud. The shear banding phenomenon is still an ongoing topic of discussion in the literature (Pignon et al., 1996, Coussot et al., 2002, Olmsted, 2008, Divoux et al., 2016, Bonn et al., 2017). Although the effects of wall slip and flow localization phenomena on grout propagation are not yet fully understood, their effects on rheological measurements have been demonstrated in several previous research works(Besseling et al., 2010, Coussot, 2005, Divoux et al., 2016, Møller et al., 2008). Their distinctive attributes, as seen from common flow curves of cement grouts, allow the extraction of approximate values of shear rates wherein their effects are prominent. For instance, research work detailing the unstable flow branch that results in the flow curves of cement suspensions due to flow localization has been described by Rubio-Hernández et al. (2018) and Qian and Kawashima (2018). In this thesis, rotational rheometry was used to further investigate such flow anomalies, intending to explain how they affect grout propagation and whether they can be parameterized for grouting design.

Besides direct rheometry of cement grouts, other fundamental experiments in the form of radial flow tests were carried out to complement the body of work on theoretical analysis of radial flow (Wallner, 1976, Dai and Bird, 1981, Lipscomb and Denn, 1984, Hässler, 1991, El Tani, 2012, Gustafson and Stille, 2005, Gustafson et al., 2013, Zou et al., 2020a). The radial flow geometry is an idealized flow configuration between two parallel disks that is often used for describing grout propagation in planar fractures. The flow configuration is an addition to regular one-dimensional (1D) flow in pipes and channels, which do not have a velocity field that varies significantly in the main flow direction (Shamu et al., 2020). Within the radial flow setup, fluid propagation is meant to resemble the case in which grout flow starts from a central injection borehole and spreads radially outward into surrounding fractures (Hässler, 1991). The flow configuration has recently received renewed interest within the grouting community, mainly due to the unresolved issues regarding the underlying assumptions as well as the shape of the velocity profile plug-flow region that forms during radial flow (Shamu et al., 2020, Hoang et al., 2021, Zou et al., 2021). Compared to analytical and numerical work, only a few experimental tests have been carried out to verify the existing theories. As such, more experimental work is still required to cover this research gap. As a first step towards addressing the current differences that exist in the literature, this thesis contributes by developing an experimental radial flow device to study the radial flow velocity field using ultrasound-based velocimetry.

1.2 Aims of the thesis

The aim of the thesis is to contribute to the existing grouting practice on cement grout rheology and a further understanding of the fundamental radial flow configuration through systematic experiments. In point form, the aims are detailed by the following objectives:

i. To investigate and understand the existence and occurrence of the critical shear rate, unstable flow and wall slip during rotational rheometry of typical cement grouts (i.e., for a selected range of water-to-cement ratios (w/c) 0.6-0.8). The effects of these flow features on rheological flow curves are to be studied using different rotational rheometry geometries, i.e., with roughened and smooth concentric cylinders (Paper I).

ii. To assess how the fitted Bingham parameters from the flow curves obtained in the tests outlined in (i) are affected by characteristic flow features; also, how to parameterize these flow features and incorporate

them into grouting design, e.g., for grout spread estimations (Paper I and II).

iii. The first objective regarding the radial flow studies is to design an experimental radial flow model for studying radial flow velocity profiles of yield stress fluids using a common model non-thixotropic YSF fluid, i.e., Carbopol 980. The radial model is to have smooth walls, provide adjustable constant apertures and a clear flow area free of obstructions (Paper III, Paper IV).

iv. To use Ultrasound Velocity Profiling (UVP) for velocimetry. The velocity profile measurements are to be carried out using different flow apertures and at different flow rates in order to get a clearer picture of how the plug-flow region is affected by both aperture and flow rate conditions (Paper III, Paper IV and Paper V). In line with this objective, a suitable method to evaluate the plug-flow region is to be developed.

v. To analyze the influence of wall slip on the measured radial flow velocity profiles. Furthermore, methods to suppress or eliminate wall slip effects are to be explored in order to obtain experimental velocity profiles that are minimally affected by wall slip (Paper IV).

vi. A final objective is to further study the measured velocity profiles with wall slip reduction carried out and compare them with analytical predictions (Paper V).

1.3 Thesis structure

The thesis is structured as follows. Chapter 2 starts by presenting a literature review and theoretical background. The literature review is made up of two parts: the first part of the review focuses on cement grout rheological measurements, and the second part is related to the radial flow experiments. Chapter 3 describes the test materials and experimental procedures. Chapter 4 then focuses on the experimental results. This is followed by Chapter 5 that briefly summarizes the main research findings by way of a summary of the appended journal papers. Chapter 6 concludes the thesis with a summary of the main conclusions and an outlook for the future of the presented studies.

Chapter 2

Literature review and theory

This chapter aims to give a short review and basic theories related to the research work. The chapter is divided into two main sections, i.e., Section 2.1 related to cement grout rheology and Section 2.2 on the radial flow configuration.

2.1 Rheological measurements of cement-based grouts

2.1.1 Importance of rheological measurements

For many years, rheology has been an essential tool to describe the flow properties of cement-based suspensions in different construction applications, ensuring that the cement suspensions possess optimal flow properties for the specific application (Greenberg and Meyer, 1963, Banfill, 2006). For cement grouting, optimal flow properties facilitate grout injection into rock fractures with minimal sedimentation whilst simultaneously allowing for sufficient time frame for the injection process, before significant hydration occurs (Håkansson et al., 1992, Håkansson, 1993, Lombardi and Deere, 1993, Stille, 2015, Shamu and Håkansson, 2019, Draganović and Stille, 2014). Different forms of rheometrical test methods exist, with the most common being rotational rheometry (Coussot, 2005, Ovarlez, 2012). However, rotational rheometers are well suited to controlled laboratory environments as opposed to the harsh field conditions. As such, simple devices such as marsh cones and flow cups are often used in the field to provide crude estimates of the cement grouts' flow properties.

More recently, advances in technology have seen the introduction of different flow visualization techniques, such as those based on Magnetic resonance imaging (MRI) and ultrasound, e.g., pulsed ultrasound velocimetry (Powell, 2008, Jarny et al., 2008, Rahman et al., 2017, Håkansson et al., 2017). Such methods provide near real-time fluid viscosity measurement, allowing rheometric measurements within the process line (in-line). For example, the work by Håkansson et al. (2017) showed how ultrasound-based velocimetry in combination with pressure difference measurements (UVP+PD) measures

cement grout rheology with the potential of being used during grouting operation in the near future. However, such systems still have to be validated in practice before their widespread use, leaving rotational rheometers as one of the few widely used and more accurate rheological test devices. In some studies, flow visualization methods are coupled to conventional rotational rheometers to obtain local velocimetry measurements in addition to macroscopic rheological measurements (Ovarlez et al., 2011, Jarny et al., 2008). Such studies have led to a greater understanding of particle migration, sedimentation, and flow localization phenomena that are otherwise overlooked during rheometric testing.

The objective of rheometry, in general, is to simplify the problem of defining the shear stress versus shear rate relationship of a fluid by making use of simple shear flow. Shear flow is achieved by the relative motion of different layers of a fluid that are placed in contact with a rotating part of the rotational geometry. For rotational rheometers, different types of test geometries are available for forming the crucial shear gap, wherein the suspension flows during rheometric testing (Banfill and Saunders, 1981, Shamu and Håkansson, 2019). A typical geometry is a concentric cylinder (Couette) geometry, which is suitable for more dilute cement suspensions, i.e., with higher water content (w/c ratios) such as cement grouts (Banfill and Saunders, 1981, Nguyen and Boger, 1992) (Figure 2.1). In most cases, the inner cylinder (rotor) is rotated at different rotational velocities that are related to the shear rate $\dot{\gamma}$ at the rotor wall r_1, whilst the outer cylinder is held stationary. In this way, adjacent fluid cylindrical fluid layers slide over one another. By measuring the resultant torque M, that is the force due to friction at a particular rotational velocity Ω, the corresponding shear stress τ at a distance r is then determined. An equation for the shear stress distribution along the shear gap given a concentric cylinder geometry with a rotor height of h is then defined by Equation 2.1,

$$\tau(r) = \frac{M}{2\pi h r^2}. \tag{2.1}$$

Equation 2.1 shows that the stress decreases from the inner cylinder r_1 to the outer cylinder r_2. In the special case where the ratio of the two cylinders is small enough, i.e., $r_2/r_1 < 1.05$, the shear stress can be considered uniform across the shear gap. Based on this assumption, the shear rate $\dot{\gamma}(r)$ can be estimated by Equation 2.2 as follows,

$$\dot{\gamma}(r) = \frac{\Omega r_1}{r_2 - r_1}. \tag{2.2}$$

Repeating the measurement process for several rotational velocities yields points that constitute a rheological flow curve, i.e., a common rheological

plot of the shear rate versus shear stress relationship of the material being tested.

As outlined in the Introduction, rheological constitutive models are then used to describe the fluid's flow curve data or rheological behavior more straightforwardly. The use of such models, e.g., the Herschel-Bulkley model, Bingham model, and Casson model, results in essential model parameters for comparing fluid properties and adjusting mix ratios to achieve the desired rheological behavior for an application. All three models feature a yield stress component τ_0. In the current work, the Bingham and Herschel-Bulkley models were primarily used and the equations describing these rheological models given the shear stress and shear rate data $(\tau, \dot{\gamma})$ are as follows: the first is the most widely used and simplest two-parameter Bingham model, with a Bingham yield stress τ_0 and a Bingham viscosity μ_B,

$$\tau = \tau_0 + \mu_B \dot{\gamma}. \tag{2.3}$$

The second one is the Herschel-Bulkley model, a three-parameter model, which has often been shown to fit the lower shear rate data of particularly of low water content cementitious suspensions in a better way compared to the Bingham model (Yahia and Khayat, 2001). The Herschel-Bulkley equation is given by Equation 2.4,

$$\tau = \tau_{0_{HB}} + k\dot{\gamma}^n. \tag{2.4}$$

$\tau_{0_{HB}}$ is the Herschel-Bulkley yield stress, k is the consistency coefficient, and n is the flow index.

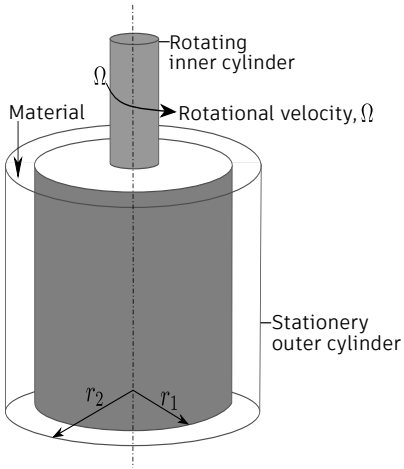

Figure 2.1 – Schematic of the concentric cylinder geometry for rotational rheological tests.

2.1.2 Complex rheological flow behavior

The rheological models outlined in Section 2.1.1 are simplistic constitutive models based on several assumptions (Frigaard, 2019). The primary assumptions include the no-slip boundary condition at the rheometer geometry walls, homogeneous shear flow is attainable at all shear rates, and the fluid's rheological properties are not time dependent. However, in reality, this is not the case. The idealized Bingham model describes the yielding of a fluid by a sharp transition; whereas, the actual case for natural fluid systems is often a complicated process, which occurs over a characteristic range of stresses (Balmforth et al., 2014). The transition from a 'solid-like' regime or a state of rest (i.e., a state with higher resistance to flow due to higher elementary particle interactions) to a 'liquid-like' regime after yielding involves complex flow phenomena with transient regimes. Such gradual transitions in fluid flow behavior have been observed even for the simplest of Yield Stress Fluids (YSFs), e.g., as observed even for a model YSF Carbopol gel (ETD 2050) over long duration start-up experiments; see Divoux et al. (2012), Bonn et al. (2017). Carbopol gels are cross-linked polymers of acrylic acid that are often used as model yield stress fluids in rheological experiments, since they exhibit negligible thixotropy and time-dependent effects; see Dinkgreve et al. (2017). One of the more common variants is Carbopol 980 from Lubrizol (Lubrizol, 2011, 2009).

Moreover, several complex flow phenomena manifest in rheometric flows of suspensions such as cement grouts. These intricate flow phenomena have been described in the rheological literature as wall slip, shear banding, shear localization, thixotropy, particle migration, and sedimentation are among the main ones (Banfill and Saunders, 1981, Coussot, 2005, Ovarlez et al., 2011, Møller et al., 2006, Moller et al., 2009, Divoux et al., 2016). Given that most of these flow phenomena are due to the intrinsic nature of cement grouts, they merit being considered in more detail. The following paragraphs briefly describe the effects that each of these flow phenomena have on the interpretation of rheological tests, particularly flow curve measurements.

Wall slip is a common flow phenomenon in YSF flows with smooth walled surfaces (Sochi, 2011). For instance, during suspension flow in a rheometer geometry with smooth walls, the concentration of solid particles decreases towards the wall whilst the liquid concentration increases. What remains near the wall is a thin slip zone of (interstitial) liquid with an overall thickness much smaller than that of the entire sample. The shear rate in this more liquid like slip layer is much higher than the rest of the sample. Additionally, the thickness of the wall slip layer can depend on factors such the size of the

flow geometry and specific roughness of the wall layer, making it a difficult to understand (Sochi, 2011). In general, if slip is ignored, the effective viscosity is underestimated Coussot (2005), Kalyon (2005). Different methods for wall slip reduction have been tried, from physical methods, e.g., surface roughening through sandblasting, attaching sandpaper to geometry walls, grooved geometries and vane tools etc. to the use of chemical treatments that alter the surface charge in a way that suppresses wall slip (Sochi, 2011).

Thixotropy is generally described as a time-dependent decrease in a fluid's viscosity due to a reversible change of the fluid microstructure during shear (Coussot et al., 2002). Consequently, the damaged structure rebuilds if the shear force (shearing action) is removed or if the available shear force is much lower than the attractive forces needed to re-establish links between elementary structural interactions. For cementitious suspensions, the structural links due to hydration are somewhat negligible immediately after mixing and intensive shearing. However, the chemical reactions that contribute to hydration can add to the structural build-up process for longer time durations, leading to irreversible structural changes. With thixotropic yield stress suspensions, one can observe flow localization in the form of shear banding and shear localization when the applied shear rate is below a threshold value. Shear banding is prevalent when the applied shear rate falls below the characteristic critical shear rate $\dot{\gamma}_c$value of the fluid. In such a case, the fluid separates into distinct bands with flowing and stationary material that arises from the instability of competition between material intrinsic restructuration and destructuration due to flow. This situation leads to unstable non-homogeneous flows that can exhibit themselves as non-monotonic flow curves Coussot et al. (1993), Coussot (2014a). This thesis also investigates such unstable regions in cement grout flow curves. On the other hand, shear localization is a form of flow localization that arises due to rheometer shear geometry constraints. For instance, for an applied rotational velocity, the resulting shear stress distribution within the Couette gap varies based on Equation 2.1. At a low enough applied rotational velocity, the shear stress distribution within the gap would be below the critical yield stress τ_0. It might be the case that shear banding and shear localization are closely coupled, since they occur within the low shear rate range.

Additionally, particle movements, e.g., through migration and sedimentation processes, are quite common during rheometric tests of suspensions in the Couette setup (Bhatty and Banfill, 1982). These particle movements are primarily dependent on the particle concentration, amount of shear and test duration (Ovarlez et al., 2012). Furthermore, other geometries such as the

vane tool seem to induce more particle migration and sedimentation (leading to higher measured shear stresses), as demonstrated in the work by Ovarlez et al. (2011).

2.1.3 Application of rheological parameters

It is often the case that the rheological parameters determined from rheological flow curves are used as part of the grouting design process. The primary purpose of doing so is to have a theoretical basis for describing the complex process of cement grout propagation in fractures (Lombardi and Deere, 1993, Carter et al., 2015, Stille, 2015).

For example, several design methods for cement-based rock grouting within the grouting community utilize the Bingham model for grout propagation estimation. Some common ones being (Grouting Intensity Number) GIN approach Lombardi (1985), Lombardi and Deere (1993), Lombardi (1996), Aperture Controlled Grouting (ACG) Shuttle et al. (2007b,a, 2008), Bonin et al. (2012), Carter et al. (2012, 2015), North American Refusal Criterion (NARC) El Tani (2012, 2013) and the Real Time Grouting Control (RTGC) method Kobayashi et al. (2008), Fransson et al. (2016), Gustafson et al. (2013). GIN, one of the earlier developed methods, has merit in providing a simple approach aiming to control the grout spread independently of fracture aperture (Lombardi and Deere, 1993). However, other authors have pointed out the inadequacy of GIN in its lack of an injection rate to monitor and control grout spread, as well as its overestimation of grout propagation lengths; see Shuttle et al. (2007b, 2008), Rombough et al. (2006), Lombardi (2007, 2008). In contrast, the ACG method has an advanced grouting scheme featuring a more detailed characterization of the site geology, including Discrete Fracture Network (DFN) modeling and subsequent grout mix sequencing to achieve the required pressure and flow control (Carter et al., 2015). NARC emphasizes the flow rate limit as a critical parameter that arises from its central idea of having a minimal flow criterion that stands as a specification to stop grouting (El Tani, 2012, 2013). Like NARC, the RTGC and ACG methods also provide analytical tools to estimate grout propagation for a particular grouting stage or desired target. In addition, RTGC allows for the specification of flow rate and time-based stop criteria for determining the onset of flow stoppage, i.e., signifying the end of grouting. In Sweden, the focus has been on the RTGC method, having been successfully validated in some grouting projects Stille (2015). Nevertheless, any developments that arise from work related to the RTGC method can be adapted to other grouting approaches since they also use the conventional Bingham model.

To a more considerable extent, the assumption of cement grouts as 'Bingham fluids' has thus far facilitated the development of simplified analytical tools for rock grouting design. However, from a practical standpoint, the current use of the Bingham model throughout the design phase has several shortcomings that merit being more systematically addressed. Nevertheless, the Bingham model does not consider the known key shear rate aspects of cementitious suspensions, e.g., wall-slip, thixotropy, and time dependency as outlined earlier in Section 2.1.2. These shear rate aspects influence the flow behavior and thus the grout propagation, especially at low shear rates. In this way, the consequences of not considering such crucial phenomena while aiming for simplicity in design remain relatively unknown. The current thesis shows how considering the shear rate aspects and stop criteria with the Bingham model can be better used for grouting design, e.g., by presenting a derivation of the wall shear rate variable $\dot{\gamma}_{wall}$ that can be used together with the shear rate parameters $\dot{\gamma}_c$ and $\dot{\gamma}_{ns}$. By using these parameters together, grout propagation estimations could be made more reliable. The equations describing $\dot{\gamma}_{wall}$ and its dimensionless equivalent $\dot{\gamma}_{D_{wall}}$ based on RTGC variables are also summarized in Equations 2.5–2.6. These wall shear rate variables ($\dot{\gamma}_{wall}$, $\dot{\gamma}_{D_{wall}}$) are also presented as part of a single unified nomogram, facilitating their use for scoping calculations, e.g., by grouting practitioners. Only the final forms of the shear rate and flow rate equations are given in Equations 2.5–2.8. The radial flow schematic in Figure 2.2 is used as a reference; since these equations assume radial flow of cement grouts, which is subsequently discussed in Section 2.2.

The dimensionless wall shear rate $\dot{\gamma}_{D_{wall}}$ can be directly expressed in terms of the relative propagation length I_D, $\gamma = I_{max}/r_0$ the steering parameter, and the Bingham properties $\tau_0,\ \mu_B$ as,

$$\dot{\gamma}_{D_{wall}} = \left(\frac{1}{I_D} - 1\right) \frac{I_D\gamma}{1 + I_D\gamma} \frac{1}{ln(1 + I_D\gamma)} \tag{2.5}$$

$$\text{and } \dot{\gamma}_{wall} = \Gamma\dot{\gamma}_{D_{wall}}, \text{where } \Gamma = \frac{\tau_0}{\mu_B} \tag{2.6}$$

The flow rate and dimensionless flow rate are then given by,

$$Q_g = \frac{dV_g}{dt} = \frac{2I_D + 2/\gamma}{1 + 2/\gamma} \frac{(2 - 3\ I_D + \ {I_D}^3)}{\left(I_D + \frac{1}{\gamma}\right) ln(I_D\gamma + 1)} \frac{V_{g,max}}{t_0} \tag{2.7}$$

$$Q_D = Q_{gT} \frac{t_0}{V_{g,max}} \tag{2.8}$$

where $V_{g,max} = 2\pi B {I_{max}}^2 (1+2/\gamma)$ is the maximum injected volume reached at the maximum propagation length $I = I_{max}$.

2.2 The radial flow configuration

2.2.1 Importance of radial flow

Within the context of grouting, the radial flow configuration is a flow that features a fluid centrally injected from a pipe into a flow area between two parallel disks. The flowing fluid then flows radially outward from the central injection area. Such a flow configuration presents an idealization for describing two-dimensional (2D) cement grout propagation in rock fractures (Wallner, 1976, Hässler, 1991, Stille, 2015, Zou et al., 2018, Funehag and Thörn, 2018, El Tani, 2012). The basic radial flow configuration is illustrated in Figure 2.2. Since the inception of RTGC as a method for grout spread estimation, there has been a particular interest in the 2D case of radial flow (Gustafson et al., 2013, Zou et al., 2020b, Shamu et al., 2020, Stille, 2015). This interest has been partly because the radial flow geometry presents a more realistic flow configuration different to 1D pipes and channels, especially for the fractures intersecting with the injection borehole (Dai and Bird, 1981, Zou et al., 2020b).

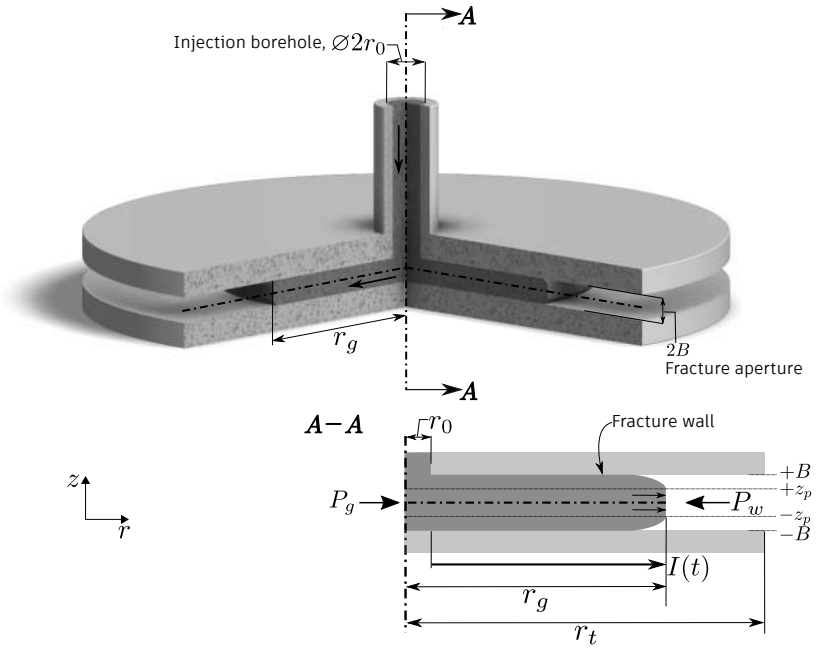

Figure 2.2 – A schematic of the radial flow configuration.

Analytical and numerical solutions have continually been developed to simplify the description of grout propagation in these different elementary geometries (both 1D and 2D) (El Tani, 2012, Lipscomb and Denn, 1984, Dai and Bird, 1981, Na and Hansen, 1967, Guo et al., 2017, Zou et al., 2020a). For the radial flow of YSFs, several analytical solutions based on the Bingham model exist (Dai and Bird, 1981, Zou et al., 2020a, Lipscomb and Denn, 1984, El Tani, 2012). More recently, renewed interest in analytical solutions to radial flow of YSFs from the grouting community has seen a discussion highlighting the main differences between the primary solutions, i.e., the solution by Zou et al. (2020a) and Dai and Bird (1981); see articles on the discussion (Hoang et al., 2021, Zou et al., 2021).

Only a few radial flow experiments are available (Savage, 1964, Laurencena and Williams, 1974, Wallner, 1976, Majidi et al., 2010, Mohammed et al., 2015, Funehag and Thörn, 2018). The majority of these experiments focused on the flow rate and pressure distributions that develop along the radial direction. The experimental work by Shamu et al. (2020) was the first study with an emphasis on visualizing the shape of the velocity flow field that emerges during radial flow. The study used Carbopol as the rheological model YSF and ultrasound velocimetry (UVP) within the constraints of an experimental radial flow device with smooth Plexiglas walls. Carbopol was used as the model YSF fluid since it exhibits minimal thixotropy and time dependency, especially for the experimental time frames in the radial flow tests (Dinkgreve et al., 2017, Bonn et al., 2017). This initial work showed detailed velocity profiles along the radial length for the first time, highlighting how wall slip affects the measured velocity profiles. Subsequent radial flow experimental studies by Shamu et al. (2021a) focused on suppressing the wall slip effects that were prevalent in the initial study by using the relatively unexplored Polyethylenimine (PEI) chemical treatment and conventional wall roughening through sandblasting Younes et al. (2020), Christel et al. (2012). The wall slip phenomenon is persistent in yield stress fluid flow, as described in the extensive reviews by (Sochi, 2011, Bonn et al., 2017, Coussot, 2014b). Thus, more detailed experimental work on YSF radial flow is required. Such work should seek to measure the 'true' shape of the radial velocity flow field with minimal wall slip effects and compare the measurements with the primary analytical solutions presented in the literature thus far.

2.2.2 Radial flow analytical solutions

In analytical solutions for YSF radial flow, assumptions such as considering a much longer main flow direction compared to the vertical aperture, no-slip wall condition, incompressible flow, steady-state, and laminar flow have been

primarily used to simplify the governing equations (Lipscomb and Denn, 1984, Dai and Bird, 1981, Park, 2020, Muravleva, 2017). The discussion initiated by Hoang et al. (2021) and the subsequent reply by Zou et al. (2021) served to highlight the differences and clarify the confusion between the leading radial flow analytical solutions for Bingham fluids presented in the literature thus far, i.e., the original solution by Dai and Bird (1981) and the one by Zou et al. (2020a).

As highlighted by Hoang et al. (2021), the fundamental differences between the two solutions are as follows:

i. The solution by Zou et al. (2020a) assumes that the vertical component of velocity in the continuity equation is negligible, whereas the solution by Dai and Bird (1981) does not make this assumption. This makes the theoretical model byZou et al. (2020a) simpler than Dai and Bird (1981); thus, making it a simpler for practical approximations related to rock grouting applications; see Zou et al. (2021).

ii. The solution by Zou et al. (2020a) applies a shear stress boundary condition where the shear stress is equal to the yield stress, i.e., $\tau_{rz}|_{z=z_p}$ within the unyielded region, the shear stress can be any value below the yield stress.

The radial flow velocity profile equations adapted to the Herschel Bulkley rheological model are described by Equations 2.9 to 2.12. Instead of the Bingham model, the Herschel Bulkley model was used since it better describes the lower shear rate rheological behavior of YSFs, e.g., the Carbopol model YSF used in the radial flow experiments. Complete derivations leading to the final form of the velocity profile equations given here can be found in Zou et al. (2020b), Shamu et al. (2020). The boundary conditions for the equations are illustrated in Figure 2.2 and the fluid is assumed to be incompressible, with negligible inertial effects. The velocity profile is then defined as,

$$v_z^f\left(z_p < z \leq B\right) = \frac{n}{n+1}\left(-\frac{1}{k}\frac{\partial P}{\partial r}\right)^{\frac{1}{n}}\left[(B-z_p)^{\frac{n+1}{n}} - (z-z_p)^{\frac{n+1}{n}}\right] \quad (2.9)$$

where v_z^f is the velocity for the yielding flow parts between the edges of the plug-flow region z_p and the walls at B, v_z^p is the velocity for the plug-flow region, and $\frac{\partial P}{\partial r}$ is the pressure gradient. The Herschel Bulkley parameters

are τ_0, k, n. The plug-region of the velocity profile is given by,

$$v_z^p\left(0 \leq z < z_p\right) = \frac{n}{n+1}\left(-\frac{1}{k}\frac{\partial P}{\partial r}\right)^{\frac{1}{n}}\left(B - z_p\right)^{\frac{n+1}{n}}. \tag{2.10}$$

Half of the plug-flow region at point z_p is expressed as,

$$z_p = \frac{\tau_0\left(r_t - r_0\right)}{\left(P_1 - P_2\right)} \tag{2.11}$$

where P_1 and P_2 are the pressure at the inlet r_0 and outlet r_t. The pressure gradient is then given by Equation 2.12 as,

$$\frac{\partial P}{\partial r} = -\frac{a_0}{r^n}, \text{where } a_0 = \frac{(P_1 - P_2)(1-n)}{{r_t}^{(1-n)} \; - \; {r_0}^{(1-n)}}. \tag{2.12}$$

The flow rate Q obtained by integration is written as,

$$\begin{aligned} Q &= \int_0^B 4\pi r \; v_z dz \\ &= \frac{4\pi r n}{n+1}\left(-\frac{1}{k}\frac{\partial P}{\partial r}\right)^{\frac{1}{n}} B^{\frac{2n+1}{n}}\left(1 - \frac{z_p}{B}\right)^{\frac{n+1}{n}}\left[1 - \frac{n}{2n+1}\left(1 - \frac{z_p}{B}\right)\right] \end{aligned} \tag{2.13}$$

It is noted here that in the case where the vertical velocity is included in the first-order approximation for 2D radial flow as pointed out by Hoang et al. (2021), the equation for half of the plug flow region changes, that results in,

$$z_p = -\tau_0\left(\frac{\partial P}{\partial r}\right)^{-1} \tag{2.14}$$

In this case, half of the plug flow region depends on the radius since the pressure gradient is a function of r, whereas half of the plug flow region in the solution by Zou et al. (2020a) is independent of the radius r since it neglects the vertical velocity. The analytical solution for the flowrate has the same form as Equation 2.13, whereas the pressure gradient needs to be inversely solved from equation 2.13 with a given boundary condition of constant flowrate Q. The wall slip that is often observed in most experiments with smooth walled geometry can be considered by using the Navier slip law (Kim, 2019, Ferrás et al., 2012, Damianou and Georgiou, 2014). In that case, v_w is the slip velocity at the wall and is proportional to the wall shear stress, i.e., $v_w = \beta\tau_w$; β is a slip coefficient. The corresponding velocity profile equations after considering wall slip are then given by,

$$\begin{aligned} v_z^f\left(z_p < z \leq B\right) = \frac{n}{n+1}\left(-\frac{1}{k}\frac{\partial \mathrm{P}}{\partial r}\right)^{\frac{1}{n}}\left[\left(B - z_p\right)^{\frac{n+1}{n}} - \left(z - z_p\right)^{\frac{n+1}{n}}\right] \\ + \beta\left[\tau_0 - \frac{\partial P}{\partial r}\left(B - z_p\right)\right] \end{aligned} \tag{2.15}$$

$$v_z^p\left(0 \leq z < z_p\right) = \frac{n}{n+1}\left(-\frac{1}{k}\frac{\partial P}{\partial r}\right)^{\frac{1}{n}}\left(B - z_p\right)^{\frac{n+1}{n}} + \beta\left[\tau_0 - \frac{\partial P}{\partial r}\left(B - z_p\right)\right] \tag{2.16}$$

The flow rate equation with the slip term is expressed as,

$$\begin{aligned} Q &= \int_0^B 4\pi r\ v_z dz \\ &= \frac{4\pi r n}{n+1}\left(-\frac{1}{k}\frac{\partial P}{\partial r}\right)^{\frac{1}{n}} B^{\frac{2n+1}{n}}\left(1 - \frac{z_p}{B}\right)^{\frac{n+1}{n}}\left[1 - \frac{n}{2n+1}\left(1 - \frac{z_p}{B}\right)\right] \\ &+ 4\pi r B\beta\left[\tau_0 - \frac{\partial P}{\partial r}\left(B - z_p\right)\right]. \end{aligned} \tag{2.17}$$

2.2.3 Ultrasound velocimetry in radial flow

In this thesis, the Ultrasound Velocity Profiling (UVP) method is used to measure and investigate the radial velocity flow field. UVP has been used to measure velocity profiles in a wide range of complex fluids (Satomura, 1957, Takeda, 1991, Baker, 1970, Wiklund and Stading, 2008, Birkhofer, 2011, Takeda, 2012, Rahman et al., 2017). UVP works on the principle of detecting frequency shifts between successive reflected ultrasound pulses that would have been transmitted into the medium under study in a programmed way. Depending on the flow configuration, pulses received from different depths are processed using signal processing algorithms, transforming the measured frequency shifts into velocities that constitute the velocity profile (Barber et al., 1985, Jensen, 1996). The individual velocities v_i at each point of the flow geometry where the velocimetry is carried out are calculated by Equation 2.18,

$$v_i = \frac{c f_{d_i}}{2 f_0 \cos\theta} \tag{2.18}$$

where f_0 is the central ultrasound transmission frequency, c is the velocity of sound, f_{d_i} the Doppler shift frequency for particles flowing at a certain distance position (i-th gate) and θ is the Doppler angle. More details regarding the UVP system used for the current work are given under Section 3.2.2.

Chapter 3

Experimental methods

This chapter deals with the materials and measurement procedures used during the different types of experiments. Section 3.1 presents the rheometric methods for the cement grout tests, followed by Section 3.2 that describes the methods for the radial flow tests.

3.1 Rheological measurements of cement grouts

Several factors that affect the interpretation and characterization of fresh cement grout rheological behavior were outlined in Chapter 2. It was pointed out that the primary factors are mainly due to cement grouts' intrinsic chemical and physical characteristics, e.g., thixotropy, structural build-up, and cement hydration at more extended time frames with their origins at the particulate level Roussel (2016). In addition, other factors that are based on the flow geometry and surface conditions, e.g., wall slip also play a crucial role in the overall rheological characterization. Carrying out rheological measurements allows one to acquire a more general description of the flow behavior due to the underlying complex flow phenomena

Before rheological tests are carried out in a controlled lab environment, the cement grout material is often mixed with a high shear rate mixer to achieve a homogeneous suspension. Such mixing follows a well-defined test protocol to ensure that the grout is fully destructured, thus maximizing reproducible and repeatable measurements (Fernandez et al., 2002, Ovarlez, 2012). Assuming that the mixing is sufficient, the subsequent flow curve measurements are also influenced by test time, temperature, and geometry wall roughness, amongst other factors (Roussel, 2005, Coussot, 2005). Previous works dealing with cement grout flow curves have not studied in detail how wall slip and flow localization affect the measured flow curves and the resulting fitted Bingham model parameters. As such, the primary factors that were systematically studied to address this research gap are as follows:

i. The effect of measurement interval t_w or duration of time allowed to attain some reasonable steady state per shear rate point during flow

curve sweeps; see Banfill and Saunders (1981), Shaughnessy and Clark (1988).

ii. The effect of different concentric cylinder geometry, i.e., different rotors and cups, as shown in Figures 3.3 and 3.4.

iii. The tests were carried out on cement grouts with different water to cement ratios typical used in grouting practice, i.e., Swedish tunneling projects. Two grout mixes were used; a thicker grout with a w/c of 0.6 and a thinner one with a w/c of 0.8.

3.1.1 Materials and preparation procedures

The preparation of cement grouts involved a mixing procedure to produce fully dispersed cement grout batches for rheological testing (Banfill and Saunders, 1981, Coussot et al., 2002, Ovarlez, 2012, Rahman et al., 2015). The mixer used to disperse the cement powder was a high shear mixer (Dispermat CV30). The total mixing time for each batch was ~4 minutes at ~10 000 rpm; the mixer is shown in Figure 3.1. Immediately after mixing, a fresh sample from the batch was poured into the rheometer test geometry. Figure 3.2) shows an image of the rheometer that was used for the cement rheological tests (TA-Instruments, 2006). When the concentric cylinder geometries shown in Figure 3.3 are setup as part of the rheometer system, the final shearing gap is then 1 mm for all cases (see Figure 3.4). In this thesis, the behavior of pure cement grouts without additives was studied.

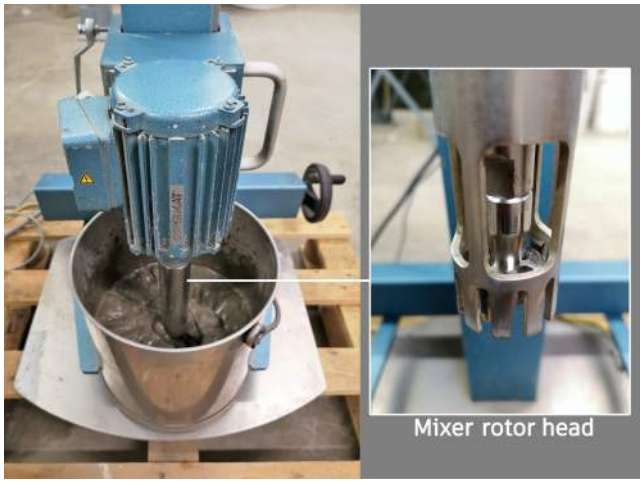

Figure 3.1 – Dispermat CV30 high shear mixer for mixing the cement grouts.

Figure 3.2 – TA AR-2000ex rheometer used for the rheological measurements

It has been shown already that the general effect of commonly used superplasticizing agents is a flow curve that qualitatively resembles the one obtained for a pure grout with the same flow w/c ratio, but with lower stress values (this means a lower yield stress and viscosity) (Håkansson et al., 1992, Wallevik and Wallevik, 2011). The Cement grouts used were prepared from Cementa Injektering 30 (CEM I 52,5 N - SR 3 LA), a common cement type that is often used in Swedish tunneling projects (Cementa, 2013).

3.1.2 Rheological test procedures

The systematic flow curve tests following the factors listed in Section 3.1 involved the following steps. Each cement mix, i.e., a fresh batch of w/c 0.6 or w/c 0.8 was tested in every one of the three available concentric cylinder geometries shown in Figure 3.4. For each flow curve test, an increasing shear rate sweep followed by a decreasing shear rate sweep were used, i.e., controlled shear rate (CSR) flow sweeps. Each flow curve test also had a time factor that was tested, i.e., the measurement interval or time per shear rate point t_w. In this way, with 3 test geometries, 2 cement mixes (w/c 0.6

and 0.8), and 3 measurement intervals t_w = 4, 24 and 40 seconds, a total of 18 flow curves tests were carried out. The shortest measurement interval of four seconds was selected to investigate whether such short time intervals had any influence on the flow curves. Also, t_w = 4 s was selected based on the fact that it had been used in previous cement grout tests (Rahman et al., 2017). The other two measurement intervals t_w = 24 s and t_w = 40 s were estimated from step shear rate tests carried out for 100 s at (0.01 and 20) 1/s to ascertain some reasonable steady state time, which was determined to be ~60 s (Paper I). For each of the 18 flow curve tests, a rheometer pre-shearing of 20 s at 300 1/s, followed by a rest of 30 s was performed. For each flow sweep the shear rate range was between 0.001 to 300 1/s, with 10 points per decade. However, only the flow curves from decreasing shear rates (down curves) were used for the Bingham fitting analysis. This is because data obtained from down curves is more representative of the grouting condition, i.e., starting from higher shear rates (near borehole) down to lower ones. Also, the down curve data is more repeatable (i.e., within 10%), compared to the up curves.

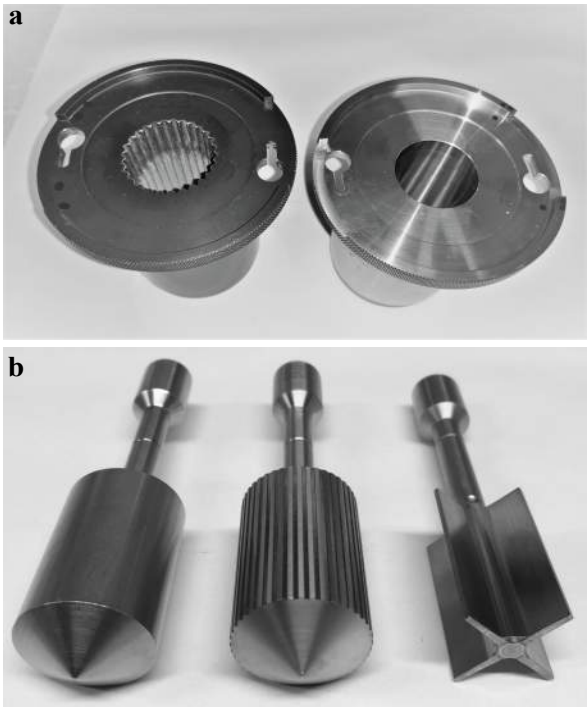

Figure 3.3 – Images of the concentric cylinder geometry, (a) grooved cup and smooth cup (b) Smooth rotor, grooved rotor, and four-blade vane

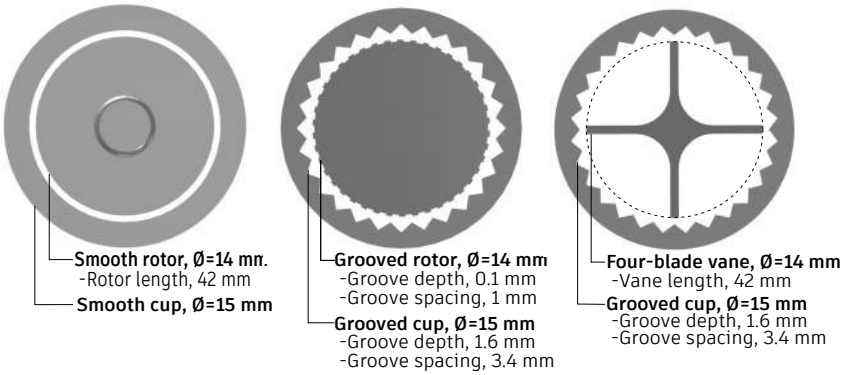

Figure 3.4 – The schematics illustrate the dimensions of the different concentric cylinder geometries used for the rheological measurements: (a) Smooth concentric cylinders (b) Grooved cup and rotor, and (c) Vane and grooved cup. The effective shear gap in all cases is ~1 mm.

Additionally, creep measurements were carried out as a further investigative step for flows at low shear rates, where unstable flows due to the critical shear rate are expected. The results of the measurements are summarized in Chapter 4 with reference to Paper I.

3.2 Radial flow experiments

A description of the radial flow model design is presented under Section 3.2.1. Following that are the preparation procedures for the yield stress model fluid, i.e., Carbopol 980 microgels. Lastly, the measurement protocols and a brief description of the ultrasound velocimetry technique are given.

3.2.1 Radial model design

The initial design of the physical radial model as presented by Shamu et al. (2020) was based on earlier models presented in the literature Savage (1964), Laurencena and Williams (1974). The objective was to have a radial flow area clear of intrusive objects, e.g., bolts, to study the underlying radial flow of Carbopol. The entire setup, including an image of the final model presented by Shamu et al. (2021a), is shown in Figure 3.5. The modifications to the original flow device by Shamu et al. (2021a) were aimed at addressing Plexiglas disk bending during high-pressure flow conditions in the smallest aperture and eliminating the wall slip effect through different wall treatment procedures. A description of the wall treatment procedures is given in Section 3.2.2.

A brief overview of some pertinent details considered in the design and assembly of the radial flow model are as follows. Figure 3.5 shows the entire radial flow device and experimental setup. The radial model design was such that a constant aperture could be achieved by a set of 8 steel spacers that separate two circular Plexiglas disks 3.6. The Plexiglas disks form the walls of the radial flow area, and each Plexiglas disk is 25 mm thick. The top disk has a machined slot that is 40 mm wide to carter for the ultrasound sensor (Figure 3.6). The slot extends from a radial length of 100 mm to 500 mm. The first 100 mm and last 100 mm of the radial length are not used for measurement to avoid possible entrance and exit effects.

Another reason for not extending the slot (thinner Plexiglas section) to the center is that the central region is normally subjected to upward bending, especially during high flow rate conditions. In order to maintain the required aperture and resist disk bending, steel structural frames are used. The top Plexiglas disk is supported by a spoke-shaped structure with a circular rim, whereas the base structural table frame supports the bottom disk. The initial spoke structure contained four frames that were attached to the top disk by bolts. The improved spoke structural frame had solid rectangular beams added between the existing ones for better reinforcement (Paper IV).

The velocity profile measurement system used was the pulsed ultrasound flow visualizer, supplied by Incipientus AB, Sweden (`https://www.incipientus.com/products/pulsed-ultrasound-flow-visualizer/`). The ultrasound parameters used during the measurements are summarized in Table 3.1. During radial flow tests, the ultrasound sensor is moved to different radial positions along a machined slot using an electronic linear axis, LEZ1 from Isel (ISEL, 2021). The resulting velocity profiles are then visualized on the control laptop, which is also used to program the linear axis. Pumping is carried out using a rotary lobe pump supplied by Colly FlowTech AB, Sweden, with fine flow rate control provided through the variable frequency drive (CollyflowTech, 2018). A magnetic flow meter Optiflux 4000 (supplied by Krohne, Sweden) was used for flow rate verification (Krohne, 2021); see Figure 3.5.

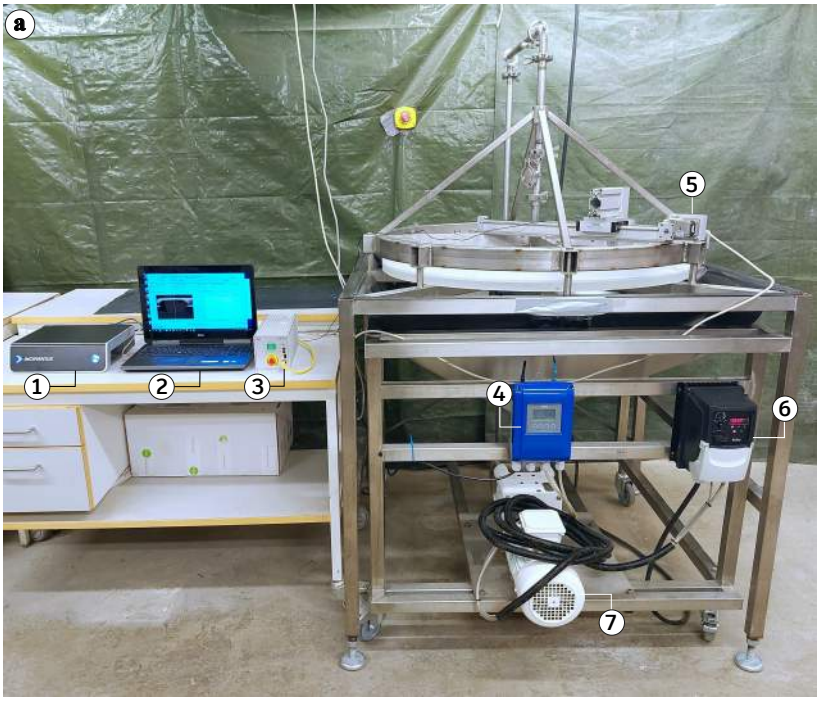

1. UVP system electronics
2. Control PC
3. Linear axis electronics
4. Magnetic flowmeter display
5. Linear axis and ultrasound sensor
6. Variable speed drive
7. Piston rotor pump

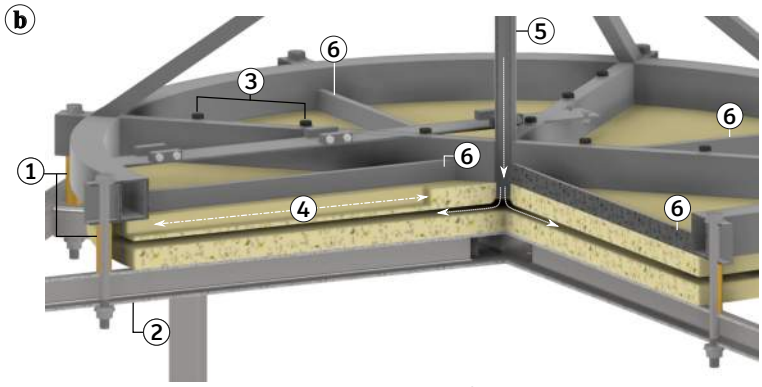

1. Stainless steel spacers
2. Base stainless steel frame
3. Bolts drillined into top disk
4. Slot for ultrasound sensor
5. Section of inlet pipe
6. New stainelss steel frames

Figure 3.5 – (a) Image of the radial flow model (b) CAD model cross-section view showing the structural configuration.

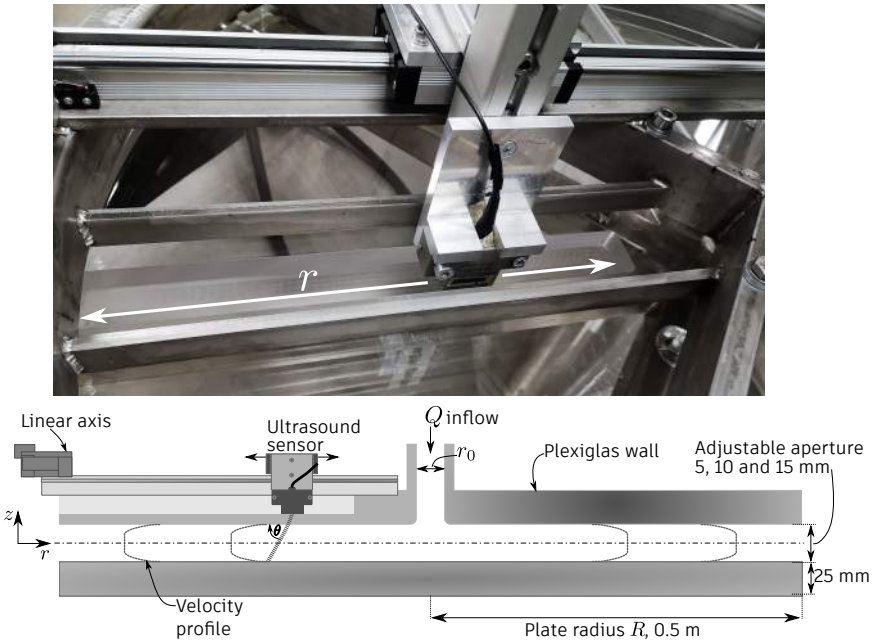

Figure 3.6 – (Top) Image showing top part of radial flow device, with the linear axis and ultrasound sensor setup (Bottom) Schematic of measurement slot and ultrasound sensor configuration.

3.2.2 Ultrasound Velocity Profiling (UVP)

Acoustic characterization

The main sensor unit of a UVP system is the ultrasound sensor itself. The accuracy of the measured velocity points that constitute a complete profile depends on how well parameters such as the beam angle (Doppler angle, θ) and velocity of sound c in the fluid are known (the schematic in Figure 3.6 shows the Doppler angle θ). The graph in Figure 3.7 demonstrates the importance of these two parameters, i.e., the curves show the expected percentage error in the individual velocity points V_{error} in a complete velocity profile, depending on the percentage error in θ, c, or their combined effect (i.e., sum of $\theta_{error} = 10\%$ and $c_{error} = 10\%$).

The curves in Figure 3.7 use the measured Doppler angle of 70.23° for the ultrasound sensor as the reference (zero error) (Table 3.1). Similar graphs for errors due to ultrasound sensor misalignment whilst assuming different reference values for the Doppler angle have also been presented by (Yamamoto et al., 2006).

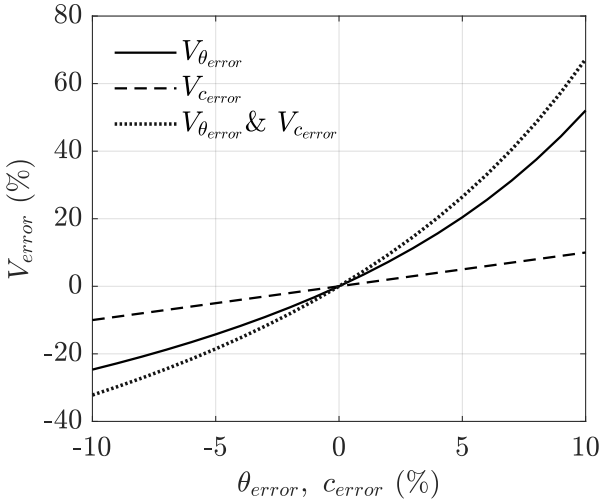

Figure 3.7 – Graph showing the relative percentage error in the measured velocity profile points due to percentage errors in the Doppler angle, velocity of sound or their sum.

For this thesis work, full acoustic characterization tests were carried out in order to accurately determine the values of θ and c. The Doppler angle tests were carried out using an advanced acoustic characterization experimental setup with a needle hydrophone. An image of the ultrasound scanning tank used for the acoustic characterization tests is shown in Figure 3.8. The acoustic tests were carried out with Plexiglas attached to the ultrasound sensor surface in order to accurately determine the Doppler angle.

The sound velocity was measured within a small stainless-steel cell of diameter of ~31 mm. A Carbopol sample at ~19 °C was placed in the cell, and then 12 pulses were transmitted into the sample. By using the Time of Flight (TOF) method, the traversing time was calculated and consequently the sound speed in all the Carbopol gels used averaged of ~1500–1520 m/s. Detailed information on the acoustic tests are described by Shamu et al. (2016) and in the appended Paper III (Shamu et al., 2020).

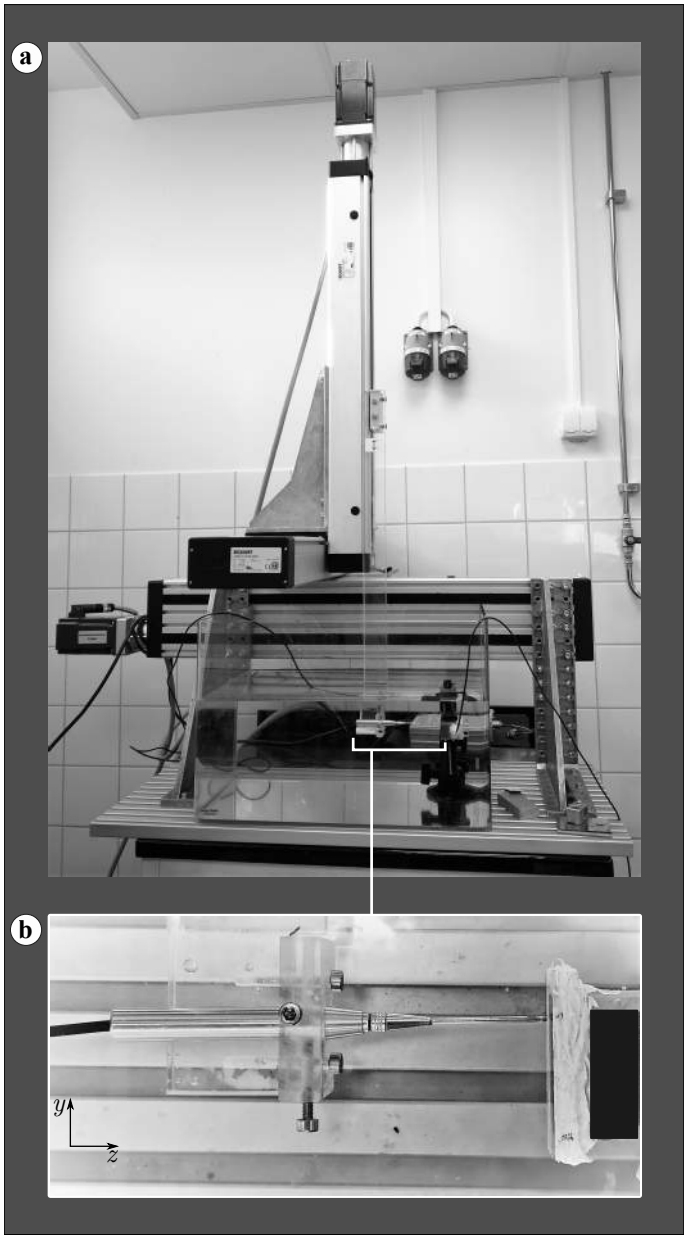

Figure 3.8 – Acoustic characterization setup to measure the Doppler angle parameter required for velocimetry (UVP). (a) 3-axis scanner to position the needle hydrophone (b) needle hydrophone scanning the surface of the ultrasound sensor; the Plexiglas sheet is glued to the ultrasound sensor.

Table 3.1 – Pulsed ultrasound measurement parameters and flow conditions for the radial flow tests

Parameter	**Value**
Ultrasound sensor central frequency, f_0	5 MHz
Number of cycles per pulse,	2
Number of pulse repetition intervals (PRI)	8192
Pulse Repetition Frequency (PRF)	0.128–1.25 kHz
Number of velocity profiles averaged	255
Gain setting (received signal)	26 dB
Transmission voltage (TX), V_{pp}	80 V
Spatial resolution (with decimation), Δz	0.028 mm
Velocity of sound in Carbopol	~1490-1510 m/s
Spectral estimation method	FFT
Flow rate conditions[a], Q	28, 40 and 55 l/min;
Doppler angle, θ	70.23°
Disk apertures, $2B$	5, 10 and 15 mm

[a]The maximum flow rate is ~58 l/min for the first set of tests (Paper III) and in Paper IV and V it is ~55 l/min.

Velocity profile plug-point detection

The plug-flow region emerges in the flow of yield stress fluids and its width is directly related to the magnitude of a fluid's yield stress. Within this region, there is negligible or zero shear between adjacent fluid layers. Most studies that present measured velocity profiles have used rheological model fitting for plug-point detection (Dogan et al., 2002, Wiklund and Stading, 2008, Rahman et al., 2015). With measured velocity profiles, some local noise fluctuations are normally present. These fluctuations interfere with the calculation of accurate plug-points (yield-points) and as such smoothing procedures, e.g., spline or polynomial fitting are normally carried out to address inaccuracies associated with the fluctuations (Arola et al., 1998). However, such fitting procedures can be strongly model dependent, complex due to several adjustable parameters, and altogether incur low reliability. As part of the radial flow studies, an algorithm based on the cumulative sum (CUSUM) was developed and used for plug-point detection (Shamu et al., 2020). The latest form of the CUSUM-based algorithm replaces the smoothing spline fit to the velocity profile with a Tikhonov regularized profile, described in an earlier study by Yeow and Taylor (2002). Figure 3.9 illustrates the regularized (Tik.) and measured velocity profiles, together with the estimated plug point (z_p, V_z^p) for a Carbopol 0.15% (by weight). Without zooming, the initial plug-region could be estimated to be much larger ~6 mm, however based on the calculation it is much lower ~5.3 mm.

An outline of the steps involved in the plug-detection algorithm are as follows:

i. A Tikhonov regularized model is first calculated for an individual velocity profile; see Paper IV for the detailed derivation steps.

ii. An initial estimate of the plug-flow region is then calculated by considering all points greater than 95% of the maximum velocity value in the regularized profile v^C_{max}, i.e., all $v^C_i \geq 0.95 v^C_{max}$; v^C_i are the regularized velocity points.

iii. The CUSUM calculation to calculate the plug-point requires a target mean $\bar{v}^p_z$ and a standard deviation σ^p_z to use in the criterion that determines if a velocity point is considered a plug-point. These two, i.e., $\bar{v}^p_z$ and σ^p_z are estimated from the initial plug in step (ii).

iv. With inputs from steps (i) to (iii), the plug-point is then estimated at a position where the lower cumulative sum L_i goes lower than the limit of 6 standard deviations ($6\sigma^p_z$). The lower sum at each point is given by 3.1,

$$L_i = \begin{cases} 0, i = 1 \\ min(0, L_{i-1} + v_{z_i} - \bar{v}^p_z - 0.5n\sigma^p_z, i > 1 \end{cases} \tag{3.1}$$

3.2.3 Preparation of Carbopol gels

The test fluids used to study YSF radial flow are Carbopol gels prepared from Carbopol 980 Lubrizol®, Belgium (Lubrizol, 2011). The basic form of Carbopol is Carbomer, a cross-linked polymer of acrylic acid, which is delivered as a white powder. In the first radial flow study (Paper III) with smooth untreated geometry walls, a single concentration of Carbopol 0.1 wt. % was used. In Paper IV and V, a thicker Carbopol 0.15 wt. % was used. The two-step process of preparing Carbopol starts with dispersing an appropriate weight of Carbopol in distilled water using a shear mixer (Silverson AX5 high shear mixer at ~1000 rpm for ~25 minutes). The dispersion is left to rest to expel air bubbles and allow complete hydration, before adding seeding particles needed for ultrasound velocimetry. A blue colorant is also added together with the seeding particles. A neutralization step completes the preparation process, and it involves adding a dilute solution of sodium hydroxide (18 wt. % NaOH) at a weight of ~2.3 times the dry Carbomer powder. The final pH after neutralization is ~6.5–7.5.

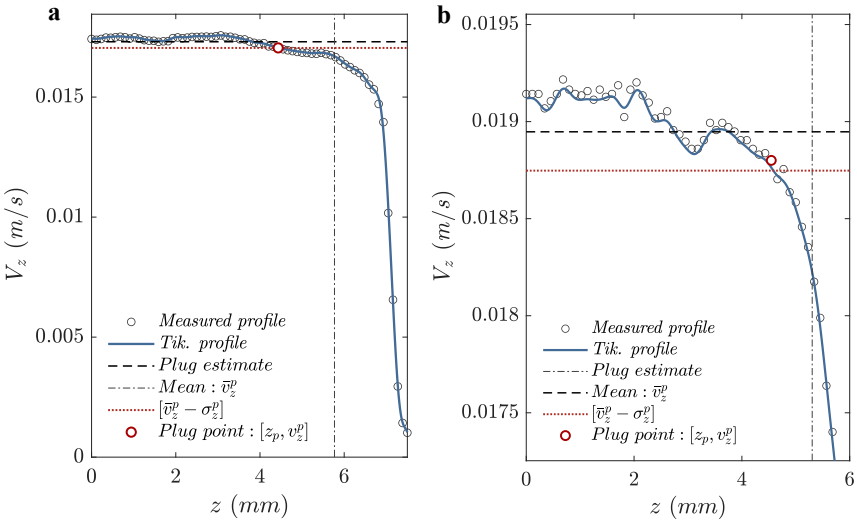

Figure 3.9 – An illustration of the CUSUM-based plug detection algorithm for Carbopol 0.15 wt. % flowing at 28 l/min and at a radial location of r = 256 mm. The wall condition is smooth and treated with PEI 0.5 wt. %. (b) Zoomed in view of (a).

The neutralization was done with a lower rpm mixer (135 rpm max.), since previous experimenters have shown that high shear mixing during the neutralization phase leads to polydisperse gels that exhibit significant rheological hysteresis (Dinkgreve et al., 2017, Di Giuseppe et al., 2015).

Example flow curves measured for some Carbopol batches used in the studies are shown in Figure 3.10. The exact values of the rheological properties used for each study are provided in the text accompanying the results in Chapter 4; see also appended Papers III–V. After the preparation and also after radial flow measurements in the flow loop, the rheology of the Carbopol was measured using a vane (15 mm diameter, 38 mm height) in cup (30 mm diameter) geometry, and at 20 °C. The shear rate flow sweeps used for flow curve measurements of Carbopol ranged from from 0.001 to 100 1/s with 10 points per decade. A time interval per shear rate point of t_w = 5 s was used in the flow curves (3.10). The first few points in each of the up-curves correspond to elastic startup effects as described by Bonn et al. (2017). The flow curves show that Carbopol exhibits simple YSF behavior that is well described by the Herschel-Bulkley model, with little to no observable rheological hysteresis.

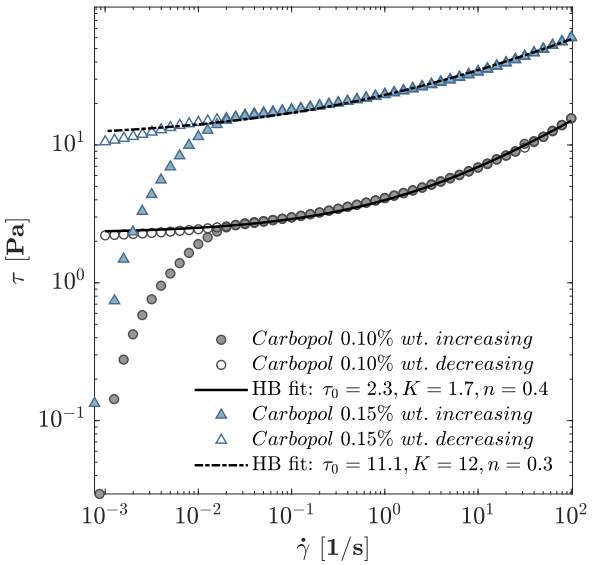

Figure 3.10 – Carbopol rheological flow curves. The first few points in the increasing flow curves are mainly due to elastic startup effects. The Herschel-Bulkley (HB) fitting was carried out on flow curves measured upon decreasing shear rates.

3.2.4 Plexiglas wall treatment for wall slip

Two different wall treatment procedures were used in order to address the significant wall slip effects observed in the first radial flow study by (Shamu et al., 2020). The first method is a relatively new procedure, in which polyethylenimine (PEI) is used to change the adhesive surface properties of Plexiglas in a way that suppresses wall slip in Carbopol gels Christel et al. (2012), Younes et al. (2020). The PEI was used at a concentration of 0.5% (by weight). Higher concentrations, i.e., PEI 2 wt. % resulted in white blob formation within the Carbopol gels. The second wall treatment is the common physical roughening procedure of sandblasting. The sandblasting resulted in a rougher Plexiglas surface characterized by the roughness amplitude, Ra ~10 µm. After sandblasting, the disks were also coated with PEI following the same procedure outlined by (Younes et al., 2020). Combining sandblasting with PEI is meant to ensure a greater probability of wall slip reduction, since some studies have shown that not all degrees of roughness eliminate wall slip (Sochi, 2011, Bonn et al., 2017).

A comparison between velocity profiles measured under the different wall conditions, i.e., completely smooth, PEI only, and sandblasted plus PEI was done to assess which method produced the most wall slip reduction. The comparison showed a similar wall-slip reduction by both treatment methods. The ratio of the wall velocity to that of the maximum in a single velocity profile was used as an indication of slip reduction. For completely smooth untreated walls, the ratio $v_{wall}/v_{z_{max}}$ was around 0.4, and with wall treatment, this ratio was ~0.1 (see Paper IV, Shamu et al. (2021a)). Based on this comparison, the PEI-only chemical treatment was then used for subsequent radial flow studies (Paper V) that required suppression of wall slip effects.

3.2.5 Test protocol for radial flow tests

A radial flow test protocol was used for each of the test conditions used throughout the radial flow studies (Papers III-V). The protocol was used to ensure reasonable repeatability and reproducibility. The steps that constitute the test protocol for the measurement of radial flow velocity profiles are as follows:

i. A newly prepared batch of Carbopol gel is placed into the tank that feeds the pump. From the tank, the fluid is pumped around the pipes and radial flow system for about two minutes to homogenize the gel and ensure a relatively steady flow rate before carrying out the measurements. A magnetic flowmeter was used to verify the steady flow rates.

ii. Once a steady flow is achieved, the ultrasound sensor attached to the linear axis is then moved to different radial locations. Velocity profiles are then measured within the radial locations 116 mm to 396 mm, i.e., in 20 mm steps.

iii. After completing measurements for each set of flow conditions, i.e., aperture and three flow rates, the steel spacers, and flow rate were then adjusted accordingly.

Chapter 4

Results

The results from the studies on cement grout rheology are summarized under Section 4.1 and those from the radial flow studies under Section 4.2.

4.1 Cement grout rheology

4.1.1 Rheological flow curve measurements

In this thesis, the focus is on flow curves measured upon decreasing shear rates, which is relevant to the actual grouting application where the highest shear rates govern the flow close to the intersecting borehole and lower shear rates farther away. Several interesting flow effects and flow features were observed in the measured flow curves, when systematic tests with varying geometry and measurement intervals) were carried out for the two types of cement grout mixes (w/c = 0.6; 0.8). All the measured decreasing flow curves are presented in Figure 4.1. The flow curves are plotted on a lin-log graph to better show the lower shear rate behavior of cement grouts. The vane geometry flow curves are always greater in shear stress magnitude than those from other geometries. The vane flow curves for both mixes are more agreeable with flow curves from other geometries, mainly at the lowest measurement interval of 4 s, and especially for the less concentrated cement grout (w/c = 0.8). These observations are explained by the vane tool's ability to reduce wall slip. However, at longer measurement intervals, i.e, t_w = 24 s and 40 s, other processes such as sedimentation and structural build-up become more leading to further increases in the magnitude of the stresses, especially at lower shear rates. Similar observations have been reported in previous studies using similar materials, e.g., cement pastes (Bhatty and Banfill, 1982, Ferron et al., 2013, Ovarlez et al., 2011). Moreover, with the vane and grooved cup and grooved cup setup the presence of secondary flow and noncylindrical streamlines that might influence the measurements is possible, as reported by Ovarlez et al. (2011). An interesting observation was that the grooved geometry could not eliminate wall slip. The slip with the grooved geometry was significant, although marginally less than that of the completely smooth rotor and cup.

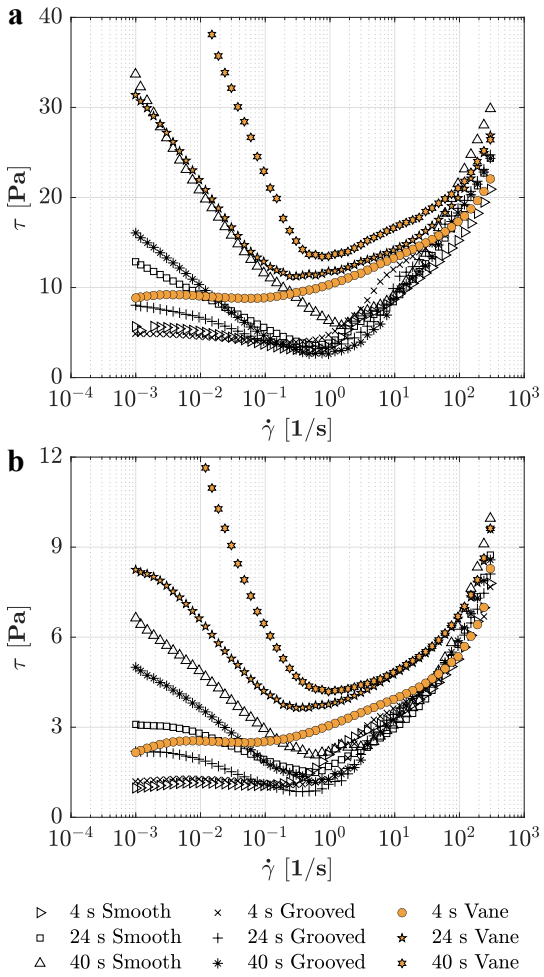

Figure 4.1 – Complete set of flow curves for cement grouts at (a) w/c = 0.6 (b) w/c = 0.8, with an unstable flow branch below the critical shear rate. Flow curves with orange symbols highlight measurements with the vane geometry.

This shows that wall slip for particulate suspensions such as cement grouts is quite complex and can be suppressed when the roughness amplitude is above a certain magnitude in comparison to the particle size. For the cement type tested, the roughness amplitude (Ra) should be above the particle size (d_{95}) of ~30 μm.

The shear rate parameters, i.e., critical shear rate $\dot{\gamma}_c$ and no-slip shear rate $\dot{\gamma}_{ns}$ could be identified. The critical shear rate $\dot{\gamma}_c$ is calculated by differentiating the flow curve and noting the point at which the slope becomes negative, and the no-slip shear rate $\dot{\gamma}_{ns}$ is taken as the point below which the flow curve has an abrupt drop (kink) in shear stress due to significant wall slip (Paper I & II). In general, below $\dot{\gamma}_c$ there is unstable flow, and a negatively sloped unstable branch of the flow curves appears. The slope of this unstable branch increases with the measurement interval t_w. Figure 4.2 is a schematic that generalizes these observations, by dividing the flow curve into three regions based on the shear rate $\dot{\gamma}$, i.e., (i) steady homogeneous flow for $\dot{\gamma}>\dot{\gamma}_c$, (ii) below $\dot{\gamma}_{ns}$ wall slip starts to become substantial, especially for smooth walled geometries, and (iii) below $\dot{\gamma}_c$ is an unstable flow region.

Paper I summarizes the fitted Bingham parameters for all the measured flow curves within two ranges of shear rates, i.e., (i) $[\dot{\gamma}_c - \dot{\gamma}_{max}]$ and (ii) $[\dot{\gamma}_{ns} - \dot{\gamma}_{max}]$. The comparison showed that Bingham fitting that does not consider wall slip ($[\dot{\gamma}_c - \dot{\gamma}_{max}]$) results in lower yield stress and higher plastic viscosity values. This analysis was the same for both w/c 0.6 and 0.8. The vane tool measurements produced flow curves that resulted in Bingham properties with the least amount of dispersion. For all tests, the range of the critical shear rate $\dot{\gamma}_c$ was ~(0.1 - 1) 1/s, whereas the no-slip shear rate $\dot{\gamma}_{ns}$ was generally between ~(1 - 10) 1/s.

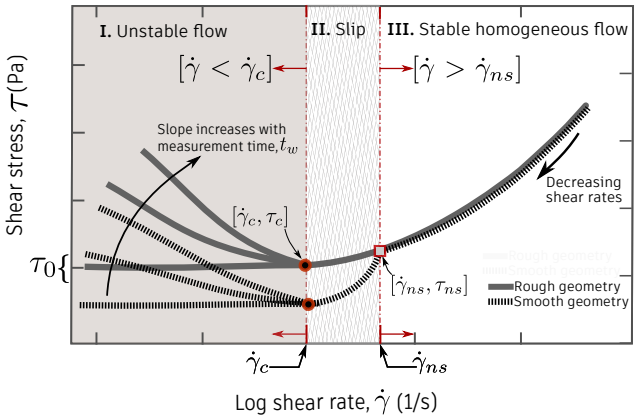

Figure 4.2 – Cement grout flow curve schematic highlighting the three flow regions based on the shear rate parameters, $\dot{\gamma}_c$ and$\dot{\gamma}_{ns}$.

4.1.2 Creep measurements

To further investigate and confirm the limits of the critical shear rate, long duration creep flow measurements were carried out. The creep tests showed that, indeed below a certain level of stress, steady flow in the form of a constant shear rate could not be achieved or maintained. Above the approximate $\dot{\gamma}_c$, it was possible to attain steady flow. The creep tests and the observation of unsteady flow below $\dot{\gamma}_c$ are in agreement with those of other thixotropic yield stress suspensions, e.g., bentonite, cements (see Coussot et al. (2006), Jarny et al. (2005).

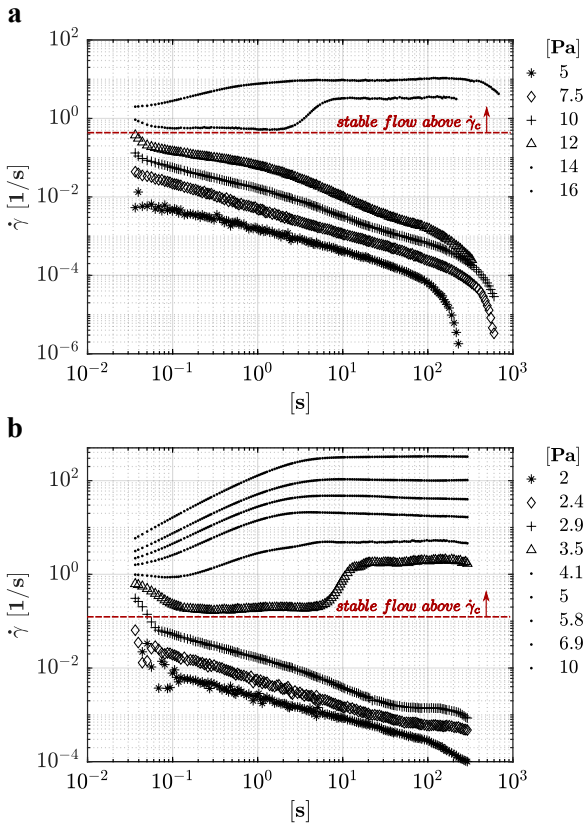

Figure 4.3 – Creep measurements for different stress levels, with (a) w/c = 0.6 (b) w/c = 0.8

4.1.3 Grouting design nomogram

The subsequent study related to cement grout rheology was detailed in Paper II. This study introduced the shear rate aspects of cement grouts as part of the grouting design while keeping the conventional Bingham model. Figure 4.4 is a flow chart that describes the steps taken to implement these design suggestions. The crucial shear rate aspects taken into account were unstable flow below the critical shear rate and wall slip, parameterized as $\dot{\gamma}_c$ and $\dot{\gamma}_{ns}$ respectively.

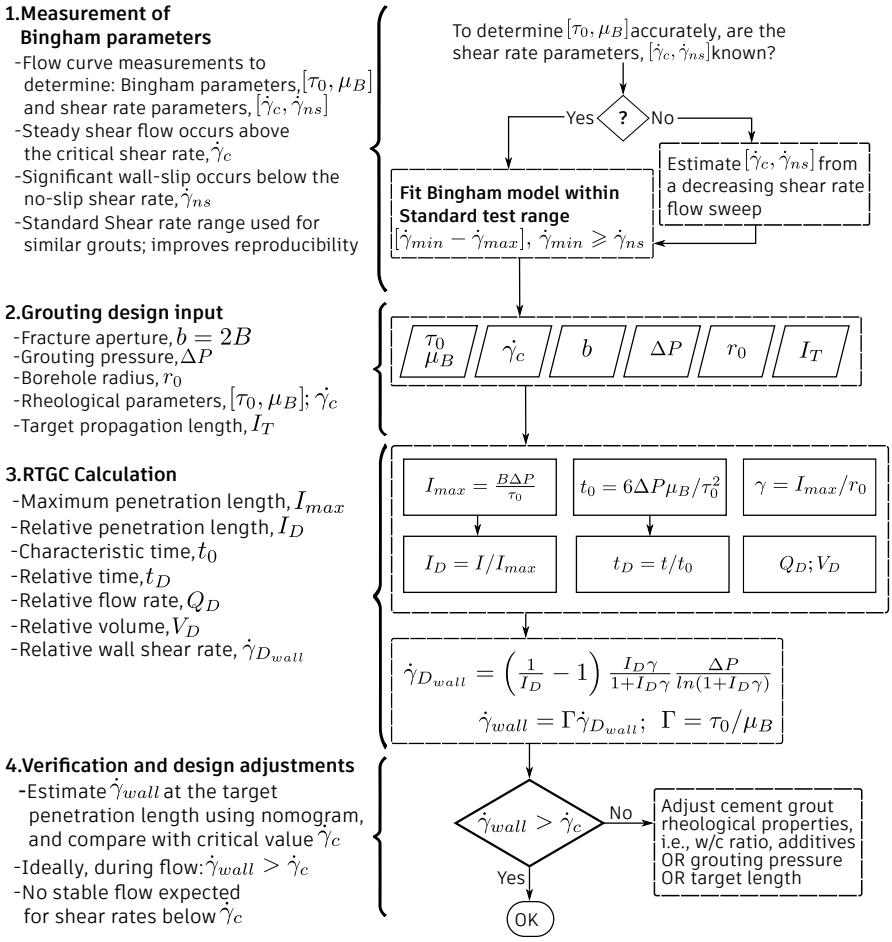

Figure 4.4 – Grouting design flow chart

All these design suggestions are meant to ensure the appropriate, and consistent use of the Bingham model for grout spread estimation, i.e., from the early stages of flow curve measurements to the actual design calculations within the RTGC framework. These changes also lead to simple practical guidelines, e.g., carrying out rheological measurements in a standardized way.

By using the wall shear rate equations described earlier in Section 2.1.3, and following the design steps in Figure 4.4 a unified design nomogram that facilitates the estimation of grout propagation was drawn up (Figure 4.5). With such a nomogram, the desired relative propagation length in dimensionless units could then be used as *input* to the nomogram (A). The other dimensionless quantities such as relative time t_D (B), relative wall shear rate $\dot{\gamma}_{D_{wall}}$ (C), and relative flow rate Q_D could then be given as *output* from the nomogram. An illustrative example demonstrating the utility of the nomogram was presented in detail in Paper II (Shamu et al., 2021b). The example made use of experimentally measured flow curves by carrying out Bingham fitting within two shear rate ranges, i.e., (i) $[\dot{\gamma}_c - \dot{\gamma}_{max}]$ and (ii) $[\dot{\gamma}_{ns} - \dot{\gamma}_{max}]$ (Region I and II, Figure 4.2). The purpose of this fitting exercise was to highlight the importance of using a well-defined shear rate range that also considers $\dot{\gamma}_{ns}$. Moreover, the final step in the design flow chart of Figure 4.4 requires a check to ascertain whether steady flow in the cement grout is prevailing at the target propagation length. This check is a comparison between the wall shear rate $\dot{\gamma}_{wall}$ calculated from Equations 2.5 and 2.6, and the critical value $\dot{\gamma}_c$ of the cement grout. The target propagation length used in the illustrative example was $I_D = 0.7$ (Paper II).

The results of the illustrative example showed that when wall slip is not considered during the Bingham fitting procedure for typical cement grouts (w/c = 0.8), the yield stress τ_0 is underestimated, whereas the plastic viscosity μ_B is overestimated. As a consequence, the grout propagation distance is overestimated by about 50%, and the overall flow rate to be monitored is actually ~50% lower compared to the flow rate considering wall slip.

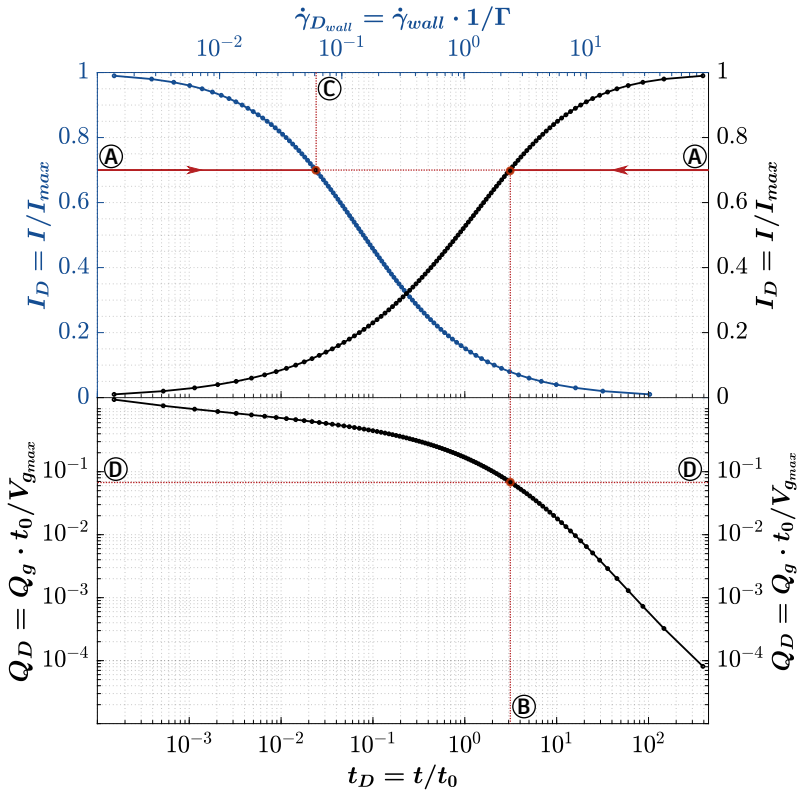

FIGURE 4.5 – Grouting design nomogram highlighting values that correspond to an input relative propagation length of 0.7 (A).

4.2 Radial flow tests

4.2.1 Radial flow: Smooth walls and wall slip

The first study on radial flow in Paper III was focused on developing a radial flow device to measure radial flow velocity profiles of a YSF, i.e., Carbopol, using the UVP technique. Apparently, this was the first time velocity profiles were non-intrusively visualized in radial flow for a YSF (Shamu et al., 2020). The complete set of measurements consists of 51 profiles per aperture, i.e., 17 different locations between radial locations $r = 116$ mm and $r = 406$ mm, at three flow rates per each of the three apertures. The wall condition was untreated smooth Plexiglas, and as such significant wall slip was observed in the measured profiles. An approximate value of the wall slip velocity was taken as the value of the velocity profile at the wall v_{wall}. Here, a subset

of the measured velocity profiles are presented, highlighting the size of the plug-flow region, the magnitude of the wall velocity, and the calculated plug points from the first version of the CUSUM-plug detection algorithm (see Figure 4.6). The measured velocity profiles are presented for the half-aperture, assuming that the velocity profile is axis-symmetric across half of the aperture. The contour velocity plots in Figure 4.6a–c are plotted from the seventeen velocity profiles measured across the radial length per flow rate and aperture condition. As expected for radial flow, the contour plots show high velocities (red area especially in the radial location ~(116-216) mm, followed by a rapid decrease in velocity magnitude with increasing radial distance.

For all the test cases presented in Paper III, the plug-points were within the range $z/B =$ 0.45 to 0.55. These plug values were higher than those predicted by the analytical solution with Navier slip (see Equation 2.11).

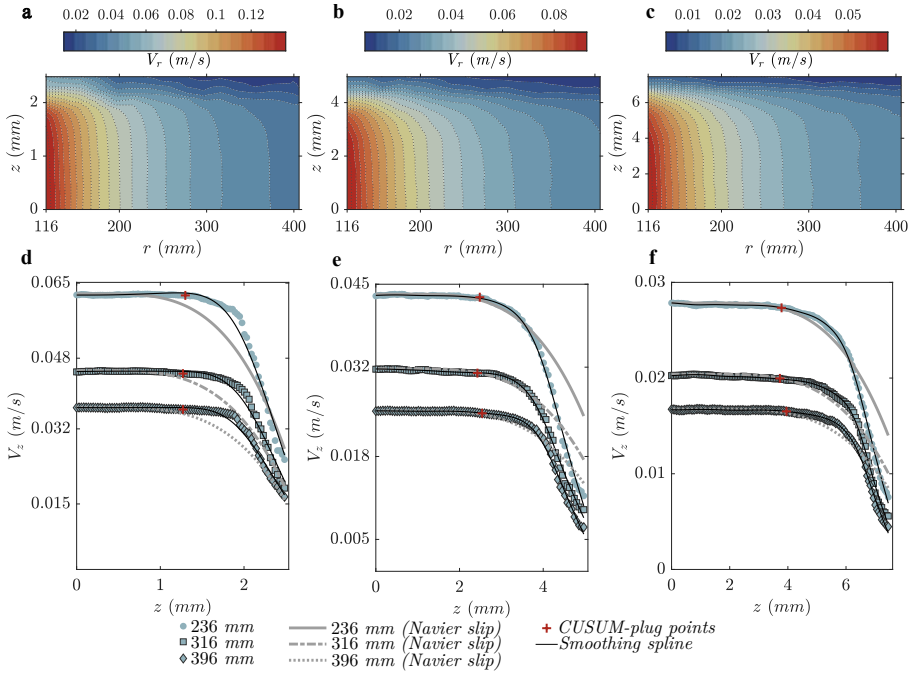

Figure 4.6 – Carbopol 0.1 wt. % velocity contour plots for the flow at 40 l/min, for apertures (a) 5 mm (b) 10 mm (b) 15 mm; the corresponding velocity profiles (d) 5 mm (e) 10 mm (f) 15 mm, with the theoretical profiles including Navier-slip. The red squares are the calculated plug-points (CUSUM method).

Since there was a flow rate discrepancy between the magnetic flow meter and the UVP calculation, especially during the high-pressure conditions, i.e., 5 mm aperture and the highest flow rate, it was presumed that disk deflection could have occurred. As such, corrections to the aperture widening were done by adjusting the nominal aperture using deflection values estimated from the Finite Element Model (FEM) simulation using the 3D CAD software (see Paper III).

4.2.2 Modifications to radial flow device

The second study on radial flow (Paper IV) focuses on developing the experimental radial flow device, making it more suitable for further radial flow investigations. Besides structural reinforcement, the new developments involved the application of different wall treatment methods, i.e., PEI at 0.5 wt. % and sandblasting (Ra ~10 μm), to suppress the wall slip effect, which makes comparisons with theoretical solutions complicated due to the assumed no-slip boundary condition (see Section 3.2.4 on wall treatment methods). Additionally, the CUSUM algorithm was modified by replacing the smoothing spline with a regularized Tikhonov function that is calculated for each measured velocity profile (Figure 4.7a). The new CUSUM method proved to be reliable for several profiles independent of radial location. The computational result of the procedure based on the average Normalized Root Mean Square Error (NRMSE) was sufficient, given that the NRMSE values of the computed velocity profiles were $< 2\%$ (see Figure 4.7).

The wall slip reduction achieved was substantial. However, the wall slip effect, i.e., non-zero wall velocities, could not be eliminated. This result is consistent with earlier work that utilized PEI (Younes et al., 2020). Figure 4.7b shows how the velocity profiles measured under untreated smooth-walled conditions compare to those from the treated walls. The wall slip reduction achieved by both PEI and sandblasting was of a similar extent, although the wall velocity ratio $v_{wall}/v_{z_{max}}$ was marginally lower with PEI. This observation was taken as a slightly better slip reduction with PEI than the sandblasting (Ra ~ 10 µm). Moreover, the plug-points determined from velocity profiles measured in the sandblasted condition had a more significant dispersion for the same flow conditions than the untreated and PEI-treated walls. This dispersion could indicate slight unevenness in the roughness along the radial length of the disks; nevertheless, wall slip, in general, is quite complex and requires further detailed study.

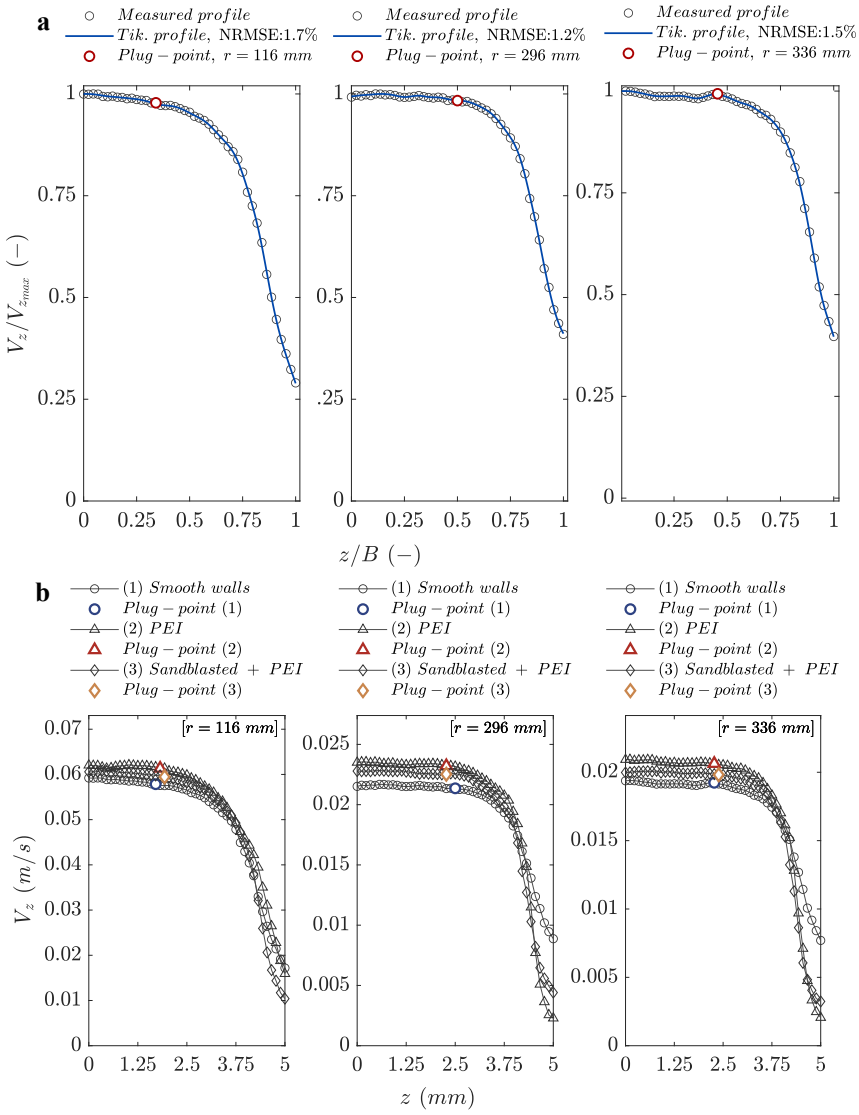

Figure 4.7 – Carbopol 0.10 wt. % velocity profiles: (a) Normalized velocity profiles at different radial positions r, within the 10 mm aperture (b) the effect of the different wall treatments at a flow rate of 28 l/min.

4.2.3 Radial flow with wall slip-reduction

After the wall slip reduction procedures of Paper IV, the final radial flow study (Paper V) focuses on comparing experimental velocity profiles with

radial flow analytical solutions for YSFs outlined in Section 2.2.2. For all measurements, the Plexiglas walls were treated with PEI. In this case, the analytical solution with a plug-flow region that is not dependent on the radial distance (Equation 2.16) and the one that depends on the radial distance (Equation 2.14) are plotted together with the measured velocity (Figures 4.8 and 4.9). A general observation from the velocity plots of Figure 4.8 and 4.9 is that there is reasonable agreement between the measured velocity profiles and the analytically predicted ones. However, in most of the cases, the measured velocity profiles are slightly lower in magnitude compared to the analytical velocity profiles. A major part of the magnitude differences are most probably caused by the persistent wall slip phenomena, which could not be completely eradicated by the PEI wall treatment procedure. Also, the magnitude discrepancy between the theoretical profiles and the measured ones is marginally higher for Carbopol 0.15 wt. % compared to Carbopol 0.10 wt. %. Another possible explanation is the more considerable wall slip effect in the thicker Carbopol due to the larger difference in viscosity between the thin 'lubricating' layer that induces slip, and the viscosity of the bulk Carbopol fluid that needs to be sheared without slip. Furthermore, other higher-order flow effects such as nonlinear flow due to inertial effects and entrance effects, as well as elastic effects unaccounted for by the theoretical model presented could play a significant contributory role in the observed discrepancies (Putz and Burghelea, 2009, Laurencena and Williams, 1974, Muravleva, 2017).

The measured plug points (z_p, V_p) as calculated by the CUSUM method are higher than those from the analytical cases. This corresponds to the expected effects of wall slip, in which the plug-region is widened in combination with reduced plug velocities (Kim et al., 2018). The magnitude difference is such that the measured plug ratios z_p/B are in some cases about ~1.5 to 2 times more than the analytically predicted ones. These plug points are further illustrated in the velocity contour plots of Figures 4.10–4.11. The contour plots illustrate the interpolated and normalized velocity field. The velocities in this case are normalized by $U = Q/Br_t$ the characteristic velocity; a similar normalization procedure was done in the recent paper by Hoang et al. (2021). In the expression for the characteristic velocity U, Q is the mean volume flow rate calculated from velocity profile integration and r_t is the radial extent of the disks, i.e, 0.5 m. The Bingham number characterizing the flow in each case was calculated as $Bn = (\tau_0/k)(B/U)^n$, where τ_0 is the yield stress, k the consistency index, n the flow index, B half the radial flow aperture, and U is the characteristic velocity. As expected, the flow conditions with the highest Bingham numbers, i.e., Bn of 0.33 to 0.44 corresponded to the slowest flows (28 l/min and 15 mm aperture).

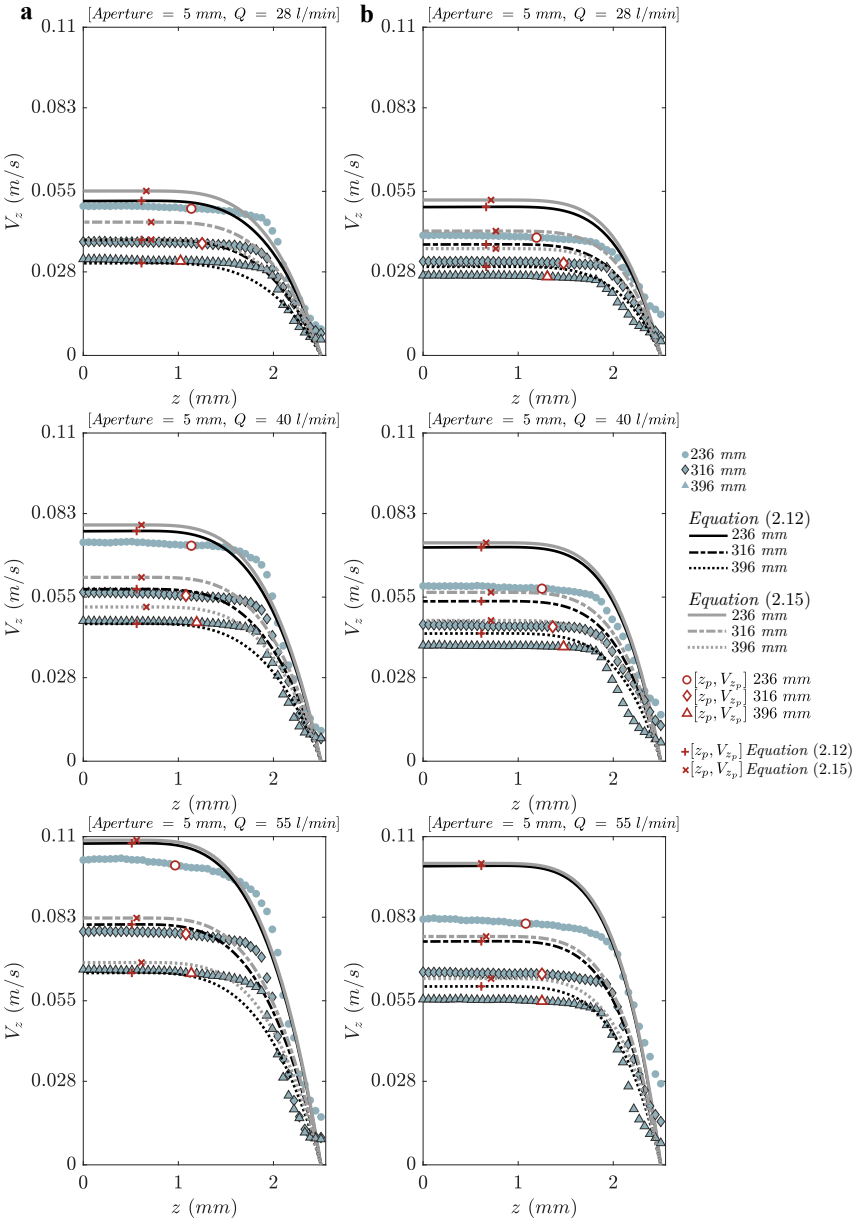

Figure 4.8 – Velocity profiles for (a) Carbopol 0.10 wt. % and (b) Carbopol 0.15 wt. %, within the 5 mm aperture at different flow rates.

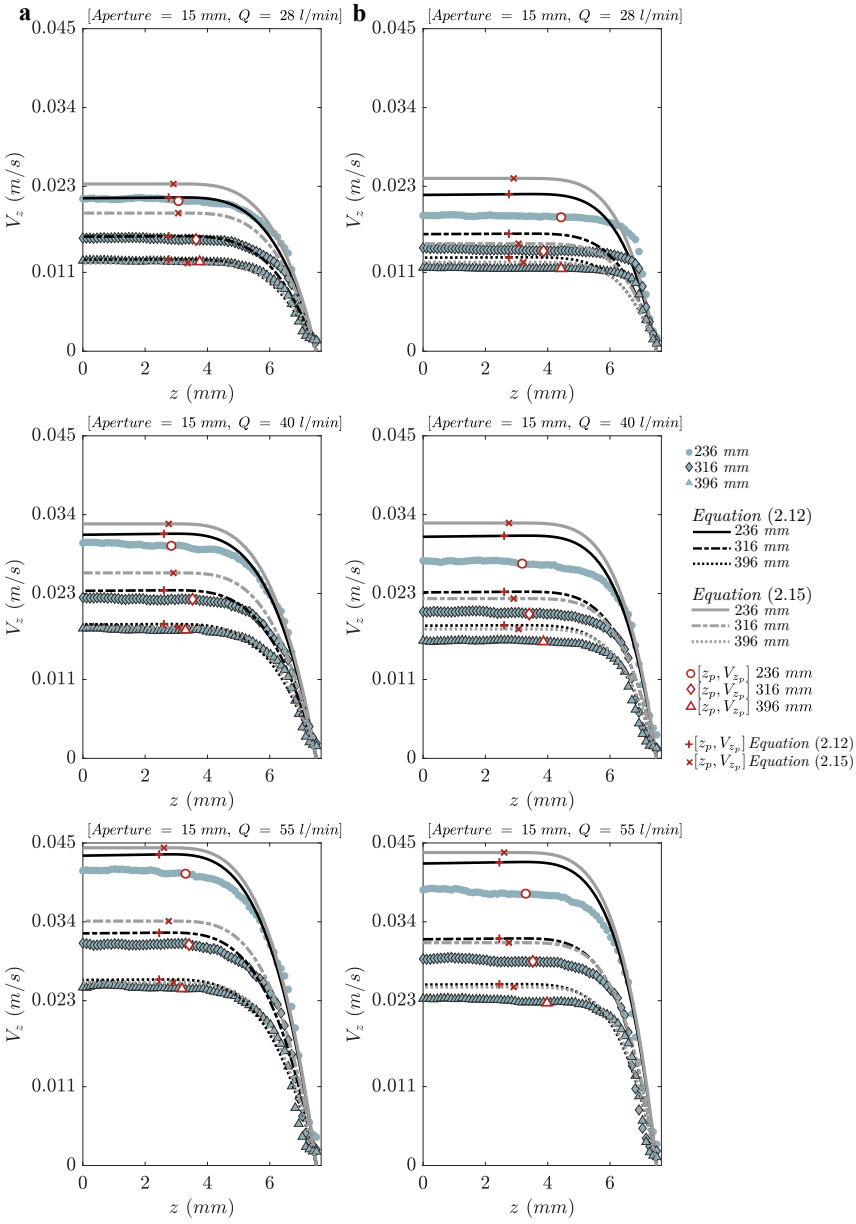

Figure 4.9 – Velocity profiles for (a) Carbopol 0.10 wt. % and (b) Carbopol 0.15 wt. %, within the 15 mm aperture at different flow rates.

A higher Bingham number indicates that the flow is dominated more by the yield stresses compared to the viscous stresses; see Ovarlez and Hormozi (2018).

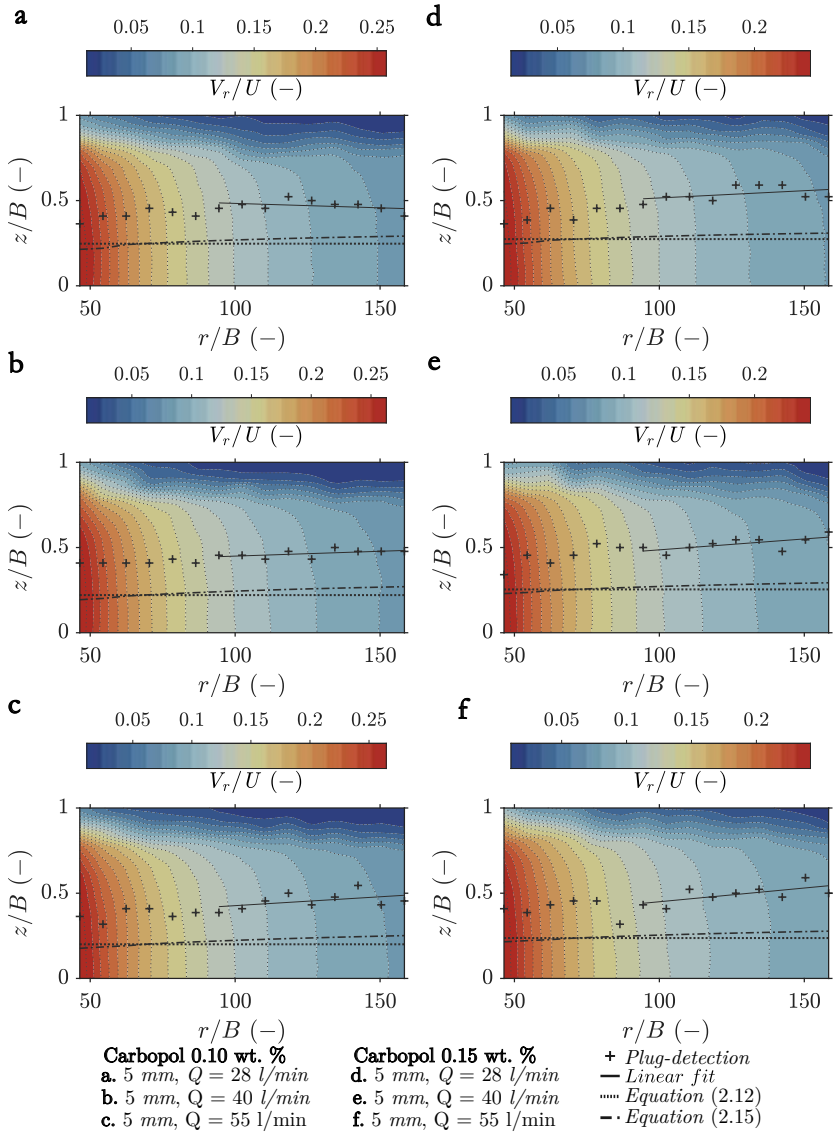

Figure 4.10 – Velocity contour plots for Carbopol 0.10 wt. % and Carbopol 0.15 wt. %, within the 5 mm aperture, and for different flow rates.

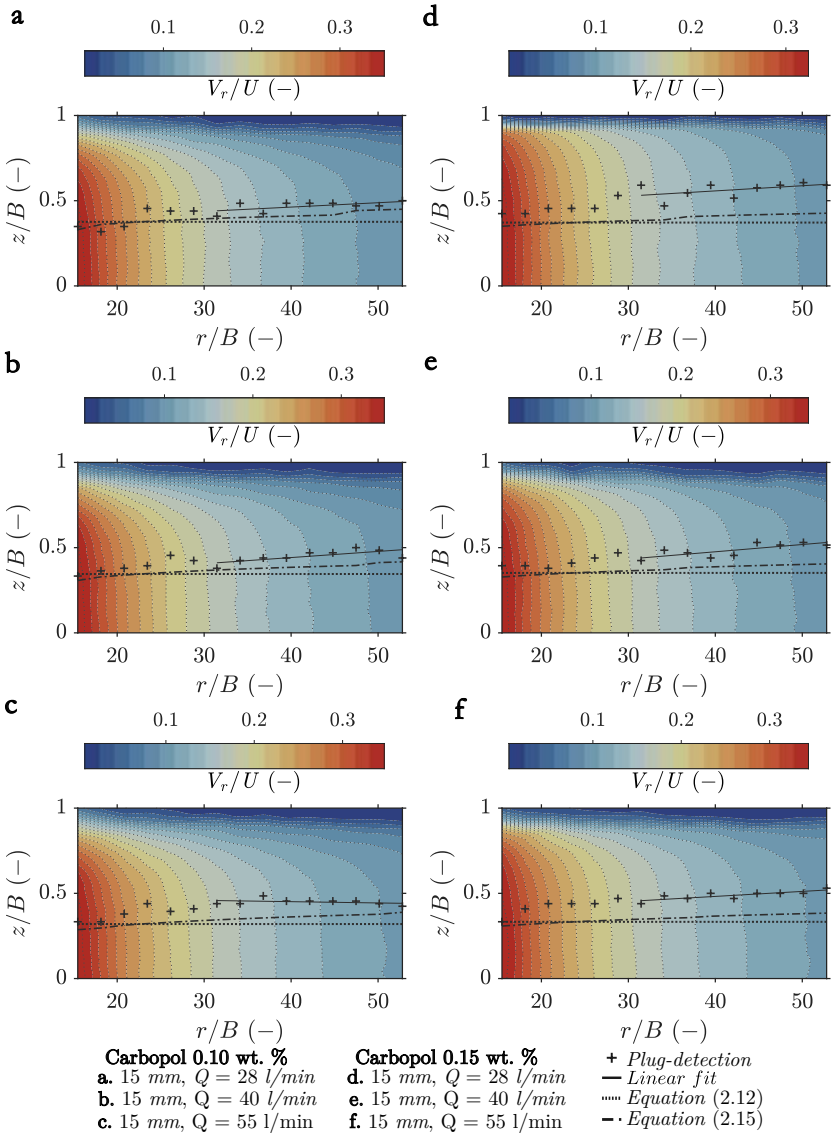

Figure 4.11 – Velocity contour plots for Carbopol 0.10 wt. % and Carbopol 0.15 wt. %, within the 15 mm aperture, and for different flow rates.

Chapter 5

Summary of appended papers

Paper I

Rheology of Cement Grouts: On the Critical Shear Rate and No-Slip Regime in the Couette Geometry

Paper I is the first of two papers (Paper I and II) that focus on measuring cement grout rheological properties and applying the determined rheological properties within grouting design. The paper presents an experimental study of the rheological flow curves of typical cement grouts. Using the controlled shear rate (CSR) mode of the TA AR2000ex rheometer, the primary factors that were studied were: (i) three measurement intervals, i.e., t_w = 4 s, 24 s, 40 s; (ii) three different concentric cylinder test geometries, i.e., smooth cup and smooth rotor, grooved cup and grooved rotor, vane and grooved cup, and (iii) two types of cement grouts (Cementa Injektering 30) with a w/c of 0.6 and 0.8. The test fluids were freshly mixed batches of a micro-cement, Cementa Injektering 30 at 20 °C.

The results showed that cement grouts are strongly shear rate dependent yield stress fluids that can be described by the Bingham rheological model but only within a specific shear rate range. It was observed that the shear rate range wherein the Bingham model is valid is primarily determined by the characteristic critical shear rate $\dot{\gamma}_c$ above which steady homogeneous flow can prevail. In addition, the measured flow curves for both cement grout mixes (w/c = 0.6 and 0.8) had substantially lowered shear stress values owing to the coupled influence of wall slip at low shear rates (<~10 1/s). This wall slip effect was more prevalent with the smooth-walled geometries. To characterize the limiting values below which the slip effects became significant compared to the vane data with minimal to no wall slip, a no-slip shear rate parameter $\dot{\gamma}_{wall}$ was used. An interesting observation was that the grooved rotor and grooved cup setup failed to eliminate wall slip; this corresponds to results from previous studies that have shown that physical roughening of any magnitude does not guarantee wall slip elimination because wall slip strongly depends on the roughness amplitude (Coussot, 2005). At present,

this dependence is not yet well understood in the literature.

The unstable flow below the critical shear rate was mainly attributed to flow localization and structural build-up. The resultant effect of unstable flow was seen by the appearance of a negatively sloped branch in the flow curve. In each case, the negatively sloped branch of the flow curve was more prominent (with a greater slope) when the vane in cup geometry was used compared to other geometries. By assessing all the flow curves, the range for the critical shear rate $\dot{\gamma}_c$ was in the range ~(0.1 – 1) 1/s, varying slightly with measurement interval and geometry. Long duration creep tests were used to complement the flow curve measurements and subsequently confirm the range of shear rates for $\dot{\gamma}_c$. It is also acknowledged that sedimentation was a contributing factor to the higher slope of the unstable flow branches in the flow curves obtained by the vane setup as mentioned by Banfill and Saunders (1981). Based on the results, some recommendations on improving the rheological test procedures for cement grouts while considering the shear rate limits $\dot{\gamma}_c$ and $\dot{\gamma}_{ns}$ were outlined.

Paper II

A nomogram for cement-based rock grouting design

Paper II continues the introductory work on cement grout rheological measurements set forth by Paper I. Paper II sought to address the limitations that come with the use of the Bingham model during rheological measurements and in the subsequent grout propagation calculations in the design phase. The primary limitations of the Bingham model were identified as being shear rate based. For instance, the key shear aspects of cement grouts, such as a critical shear rate and substantial wall slip within the lower shear rate range, are usually not considered for grouting design. As such, these shear rate characteristics, i.e., the critical shear rate $\dot{\gamma}_c$ and no-slip shear rate $\dot{\gamma}_{ns}$ were considered according to the results of Paper I. The parameterization of $\dot{\gamma}_c$ and $\dot{\gamma}_{ns}$ from rheological flow curves facilitated their incorporation into grout propagation calculations as part of grouting design. The design improvements were complemented by deriving a wall shear rate equation for the grout front in Bingham radial flow that gives the wall shear rate variable $\dot{\gamma}_{wall}$. In this way, grout flow is quantitatively described as occurring when the condition $\dot{\gamma}_{wall} > \dot{\gamma}_c$ is met; such an assessment has not been possible with the conventional use of the Bingham model. Moreover, a design flow chart was presented, illustrating how the Bingham parameters can be better estimated and subsequently used together with the shear rate parameters for grout propagation calculations. A design nomogram that simplifies and uni-

fies the grout propagation variables based on the RTGC grouting approach was developed. In the end, an illustrative example was presented to verify the suggested design improvements. One primary conclusion was that grout propagation could be overestimated by as much ~50% if Bingham fitting is incorrectly carried out using the suggested procedures that consider wall slip. The design suggestions outlined in the paper were developed within the general RTGC framework; however, they can be incorporated accordingly into other prevailing rock grouting approaches (ACG, RTGC, NARC) that use of Bingham model to describe cement grout propagation.

Paper III

Radial flow velocity profiles of a yield stress fluid between smooth parallel disks

This paper is one of three that focus on radial flow. Paper III presents for the first time an experimental device for studying the velocity flow field of yield stress fluids in radial flow by using UVP-based velocimetry. Some of the pertinent details of the experimental device include: stainless steel spoke structure with spacers on the periphery to maintain the parallel aperture between the two smooth Plexiglas disks that form the walls of the flow area, a flow area free of obstructions such as fasteners, a linear axis to position the ultrasound sensor at different radial locations, and instrumentation such as a magnetic flow meter to verify velocimetry calculated volume flow rates. Using the UVP measurement method and varying the flow conditions (aperture and flow rate), several velocity profiles were acquired to assess the dependency of the velocity profiles on the radial length and flow conditions. The conditions varied were: (i) three volumetric flow rates, i.e. 28 l/min, 40l/min, and 58 l/min and (ii) three disk apertures, i.e. 5 mm, 10 mm and 15 mm, and (iii) radial length r. A CUSUM-based algorithm was developed to accurately determine the position of the plug point (z_p, v_p) in each of the measured velocity profiles.

A general observation was that wall slip effects were prevalent for all flow rates due to the smooth-walled Plexiglas disks. The wall slip effects resulted in much larger plug flow regions compared to the theoretically predicted ones. A radial flow analytical solution incorporating the Herschel Bulkley rheological model and a Navier slip term $v_w = \beta\tau_w$ was used to describe the measured profiles. Relatively good agreement was achieved between the analytical solution and the measured profiles with the slip coefficient β = ~0.0013. However, there was some marginal disk deflection during high-pressure flow conditions within the smallest aperture. The effects of

these deflections were noticed during measurements by flow rate comparisons, and also predictions of their approximate magnitudes were determined using a Finite Element (FE) model of the radial flow area. Despite the limiting influence of the deflections, the study contributed to the limited experimental works on radial flow by showing the expected velocity profiles and the strong influence that wall slip can have during the flow of yield stress fluids.

Paper IV:

An experimental device for measuring radial flow velocity profiles of yield stress fluids

Based on the results of Paper III, Paper IV focuses on modifications to the radial flow device, improving it for further radial flow studies of YSFs. The significant modifications include (i) additional reinforcement to maintain better the required constant aperture, (ii) implementing wall slip reduction, and (iii) developing an improved velocity profile plug-detection algorithm that uses Tikhonov regularization. The additional reinforcement used solid rectangular stainless steel frames, symmetrically placed in between existing beams. Two frames were then strategically placed along the thinner Plexiglas region of the top disk where the ultrasound sensor traverses during measurements. Two methods for wall slip reduction were tested: (i) using a relatively new chemical treatment in which PEI is applied to the surfaces of the Plexiglas disks, and (ii) combining the PEI treatment with physical roughening, i.e., sandblasting the disks to a roughness, Ra ~10 μm. Both wall treatment methods provided substantial wall slip reduction; however, there were some differences in the wall velocities and plug-points measured from the different wall conditions. An assessment of these differences showed that PEI-only treatment provided slightly better slip reduction than sandblasting.

Paper V:

Radial flow of yield stress fluids: an experimental and theoretical study

Motivated in part by the recent discussions in grouting literature by Zou et al. (2020a), Hoang et al. (2021) and Zou et al. (2021) on radial flow analytical solutions, Paper V measures and compares the differences between the analytical predictions and the measured velocity profiles. This study comes after the improvements introduced in Paper IV. For this study, two concentrations of Carbopol were used, i.e., a thicker gel with higher yield stress (Carbopol 0.15 wt. %) and a less concentrated one (Carbopol 0.10 wt. %). The same flow conditions and apertures in Paper II were used for the two fluids to better assess the plug-flow region variation with Carbopol

concentration. A generally good agreement regarding velocity profile shape was achieved between the two theoretical models and the measured velocity profiles. However, there were some discrepancies in some test cases, and the measured velocity profiles had slightly lower velocity values than those from the analytical solution; the discrepancy was more considerable for the thicker Carbopol 0.15 wt. %. Moreover, the plug-points determined by the CUSUM calculation were greater than those from the analytical solutions for all flow test cases, i.e., the ratio z_p/B was greater for the experimental observations. One reason for this is the remaining wall slip that could not be eliminated. Other reasons are higher-order flow effects, e.g., nonlinear flow due to inertial effects and entrance effects as well as elastic effects, unaccounted for by the theoretical models.

Chapter 6

Conclusions and Outlook

In this thesis, two main research studies were presented. The first set of studies was on the measurement of cement grout rheological parameters and their subsequent use in rock grouting design calculations (Papers I–II). The second set of studies on radial flow were aimed at designing an experimental device for visualizing the velocity flow field of Carbopol model YSFs and comparing the measured velocity profiles with existing analytical solutions (Papers III–V).

6.1 Discussion: Cement grout rheology

By conducting systematic tests using the CSR mode of the rheometer, with three different geometries and three measurement intervals, some key features of cement grout rheological behavior were revealed in the resultant flow curves (Paper I). The flow features were characterized as being shear rate and time dependent, and these included, significant wall slip below a no-slip shear rate $\dot{\gamma}_{ns}$ and unstable unsteady flow below $\dot{\gamma}_c$. The unstable flow behavior is strongly linked to localization of flow, i.e. shear banding and shear localization, which have also been identified for other thixotropic yield stress suspensions in the literature (Olmsted, 2008, Ovarlez et al., 2009, Divoux et al., 2016, Bonn et al., 2017). In general, the critical shear rate was estimated to be in the range ~0.1–1.0 1/s for the cement grouts tested (w/c ratios of 0.6 and 0.8). This shear rate range was further supported by results from the long duration creep tests (Figure 4.3). For the geometries tested, the vane reduced wall slip significantly. However, the main drawback of the vane is probably its susceptibility to secondary flow, as well as increased structural build-up and sedimentation as a result of the stationary material in between the blades, leading to much higher measured stresses throughout the measurement shear rate range when compared to other geometries (Ovarlez et al., 2011). Surprisingly, the grooved rotor that was expected to reduce wall slip significantly could not produce the desired result (Section 4.1.1). This might be due to the inappropriate geometry wall roughness. At present, the current mechanisms that guarantee wall slip elimination are not well understood; however, the existing literature mentions that the

roughness needs to be dimensioned accordingly, i.e., greater than the particle sizes in the suspension (Coussot, 2005, Bonn et al., 2017). The subsequent study on cement grout rheology suggested a new design approach in which the shear rate aspects of cement grouts are considered, i.e., $\dot{\gamma}_{ns}$ and $\dot{\gamma}_c$. Although these shear rate aspects are relatively known, this was apparently the first time they had been parameterized and suggested for use in rock grouting design whilst keeping the common Bingham model (Paper II). Additionally, a wall shear rate $\dot{\gamma}_{wall}$ equation was derived and incorporated into a design nomogram based on the RTGC framework (Section 2.1.3). The nomogram is meant to unify all the key variables required for grout propagation estimations, assuming 2D radial flow (Section 4.1.3). The use of the suggested Bingham fitting and shear rate parameters is not only limited to the RTGC grouting approach, but can be adapted for other grouting approaches to better estimate grout propagation while keeping the Bingham model.

6.2 Discussion: Radial flow studies

The studies on radial flow described the overall design of the radial flow device for measuring radial flow velocity profiles, using Carbopol microgels as the model fluid YSFs (Paper III–V). In this way, the radial flow device using UVP for velocimetry was presented for apparently the first time, showing visualized velocity profiles of the Carbopol YSFs (Paper III). Previous experimental studies on radial flow have mostly focused on the flow rate and pressure distributions, and the propagation of the grout front, but not detailed velocity profiles (Wallner, 1976, Laurencena and Williams, 1974, Majidi et al., 2010, Mohammed et al., 2015, Funehag and Thörn, 2018). The initial radial flow tests (Section 4.2.1) showed substantial all slip effects in the velocity profiles, and this was described by a Navier slip term (Sochi, 2011, Damianou et al., 2016, Kim, 2019). The second radial flow study (Paper IV) carried out further developments on the radial flow device, i.e., reinforcement of the flow area and wall slip reduction procedures (sandblasting and PEI). An additional improvement was on the plug point detection algorithm, which utilized the Tikhonov regularization procedure by Yeow and Taylor (2002). The wall slip reduction was substantial; however, the wall slip effects could not be completely eliminated, some similar results have been presented by Younes et al. (2020) but on a much smaller scale (micro-channel). In the last study on radial flow, the analytical solutions that have been discussed in the grouting literature by Hoang et al. (2021), Zou et al. (2021) were compared to the measured velocity profiles after wall slip reduction (Paper V). A generally good agreement in terms of velocity profile shape was achieved, but with some velocity magnitude discrepancies

(Section 4.2.3). The determined plug flow regions were still larger than those calculated from the analytical solutions. These discrepancies were in part attributed to the remaining wall slip and other higher-order flow effects not considered by the analytical solutions. Earlier radial experiments with Carbopol have also suggested the possibility of elastic effects that could also contribute to the shape of the measured velocity profiles (Laurencena and Williams, 1974). However, such magnitude differences could be considered reasonable for scoping calculations during grouting design and execution (Zou et al., 2021). Overall, the results from the radial flow tests suggest that it could be worthwhile incorporating the critical features of wall slip, i.e., increased wall velocities and plug-flow regions in propagation models for cement grouts that use rheological models, e.g., the Herschel-Bulkley model (Kim, 2019). Adapting grout propagation design calculations in this way would allow more realistic modeling for the widespread case of water-filled rock fractures, where wall slip is most likely prevalent.

6.3 Conclusions

The main conclusions from this thesis are summarized as follows:

i. The flow curves of cement grouts show a significant dependency on the measurement interval t_w and Couette geometry that is used, particularly at low shear rates. By evaluating the flow curves, certain shear rate parameters such as the critical shear rate $\dot{\gamma}_c$ and no-slip shear rate $\dot{\gamma}_{ns}$ were obtained. Depending on the rheometer geometry, these shear rate parameters separate the flow curve into regions with homogeneous steady flow, significant wall slip, and unstable flow below $\dot{\gamma}_c$. The vane tool reduces wall slip; however, it might not be suitable for long duration tests were structural build-up and sedimentation dominate. Also, not all magnitudes of roughness can eliminate wall slip, as seen from the flow curves obtained with the grooved rotor. Another issue with the vane is that it can induce secondary flow at the vane blades, depending on the nature of the test fluid and magnitude of applied shear rate. Such dependencies of wall slip effects on different Couette geometries, including the vane tool, leads to Bingham parameter differences. These magnitude differences were assessed and presented in Paper I.

ii. The shear rate parameters $\dot{\gamma}_c$ and $\dot{\gamma}_{ns}$ were also parameterized and used in an illustrative example to show how wall slip due to different rheometer geometry (smooth, rough) can affect the estimated Bingham properties and in turn the estimated propagations lengths. At the same time, a unified grouting design nomogram that links important steering

parameters in dimensionless form is presented as part of Paper II. The nomogram links RTGC variables such as the relative propagation length I_D, relative time t_D, the newly derived relative wall shear rate $\dot{\gamma}_{D_{wall}}$ and the relative flow rate Q_D. Such a nomogram facilitates rapid parameter estimation in a way that can readily be used by grouting practitioners. An illustrative example presented together with the nomogram shows that, in essence if wall slip is not considered, up to 50% overestimation of grout propagation distance results.

iii. A radial flow experimental device was designed and manufactured to study the radial flow velocity field. The initial radial flow model had smooth walls and was used in a study that presented, for the first time, radial flow velocity profiles as measured by the UVP method. In general, the velocity profiles agreed well with the theoretical analytical solution that includes a Navier wall slip term (Paper III).

iv. Radial flow measurements were carried out for different flow apertures, flow rates and Carbopol concentrations in order to assess the influence of these factors on the velocity profiles. To estimate the plug-flow region of the velocity profiles, a CUSUM-based method for plug-point detection was developed as part of this thesis. The method proved to be reliable and robust enough for detecting the plugs in non-smooth velocity profiles. The method was further improved as part of Paper IV, where the smoothing spline was replaced with Tikhonov regularization.

v. The wall slip effects that appear in radial flow are addressed in Paper IV. The results from the paper showed that wall slip can be greatly reduced by using the relatively new PEI chemical treatment procedure. Consequently, the measured velocity profiles with wall slip reduction had reasonable agreement with the analytical solutions (Section 4.2.3). The ratios of the wall velocities to the maximum axial velocity $v_{wall}/v_{z_{max}}$ ranged from ~0.25–0.40 with smooth untreated walls; whereas with wall slip reduction, the ratio reduced to ~0.10.

vi. For the radial flow study with wall slip reduction, the calculated plug-points from the measured velocity profiles were larger than those predicted by the analytical solutions (Paper V). Such discrepancies are explained by the fact that the wall slip reduction was substantial, but the PEI-treatment procedure did not entirely eliminate wall slip. Moreover, it is reasonable to assume that other flow effects (entry effects, elastic effects and non-linear inertial effects) not considered by the analytical solutions could have contributed to these discrepancies.

6.3.1 Future outlook

This thesis could certainly benefit from improvements and developments in ultrasound technology, including other improved test methods, to better understand the different aspects of cement grout rheology and YSF flow in relation to grouting in real fractures. Some suggestions for future work are as follows:

- A more detailed study of cement thixotropy aimed at developing more realistic models that also include the coupled effects of wall slip to describe cement grout flow would complement the current work. The developed models can then be implemented, e.g., in numerical simulation schemes to predict with greater accuracy the expected flow conditions.

- In addition to studying the flow phenomena that affect cement grout flow properties with the use of offline methods, it is also necessary to further investigate and develop in-line rheometric methods, e.g. based on the UVP technique (Håkansson et al., 2017). With such methods, the capability for continuous digital monitoring would allow improved quality control of grouts during the grouting process. Moreover, reduced field pretesting of rheological properties would be more sustainable in the long run due to reduced cement waste from the large test batches that are used.

- Other measurement techniques not considered in the current work could be introduced as part of future work. For instance, for rotational rheometry of cement grouts, imaging and flow visualization techniques could then complement the conventional rheometry and track the particle concentrations. Incorporating such visualization techniques, especially for the vane in cup geometry, aids in explaining some obscure details, e.g., during vane measurements where sedimentation and particle migration are most likely to occur; see Ovarlez et al. (2011).

- Future YSF radial flow studies could benefit from experimental models with much larger aspect ratios than the ones presented in this work, i.e., r/B much greater than a maximum of ~158. This could be better achieved by having a smaller aperture (1 mm or less) and using higher frequency ultrasound sensors (offering higher spatial resolution >10 MHz). However, having larger scale models with diameters much larger than one meter has its own challenges, i.e., a much larger area to be reinforced, space constraints. Nevertheless, with advances in

ultrasound velocimetry as well as other velocimetry techniques, such experiments are indeed possible.

- Adapting more advanced rheological models that can better describe the critical features of YSFs, including wall slip at the geometry wall in complex flow configurations such as radial flow or roughened geometries, would also benefit the practical understanding of YSF flow in real rock fractures.

Bibliography

D. F. Arola, R. L. Powell, G. A. Barrall, and M. J. McCarthy. A simplified method for accuracy estimation of nuclear magnetic resonant imaging. *Review of Scientific Instruments*, 69(9):3300–3307, Sept. 1998. ISSN 0034-6748, 1089-7623. doi: 10.1063/1.1149113.

D. W. Baker. Pulsed Ultrasonic Doppler Blood-Flow Sensing. In *IEEE Transactions on Sonics and Ultrasonis*, volume 17 of *3*, pages 170–185, July 1970.

N. J. Balmforth, I. A. Frigaard, and G. Ovarlez. Yielding to Stress: Recent Developments in Viscoplastic Fluid Mechanics. *Annual Review of Fluid Mechanics*, 46(1):121–146, Jan. 2014. ISSN 0066-4189, 1545-4479. doi: 10.1146/annurev-fluid-010313-141424.

P. Banfill and D. Saunders. On the viscometric examination of cement pastes. *Cement and Concrete Research*, 11(3):363–370, May 1981. ISSN 00088846. doi: 10.1016/0008-8846(81)90108-3.

P. F. G. Banfill. Rheology of fresh cement and concrete. *Rheology reviews*, 2006:61, 2006.

W. D. Barber, J. W. Eberhard, and S. G. Karr. A new time domain technique for velocity measurements using Doppler ultrasound, 1985.

H. A. Barnes. The 'Yield Stress Myth?' Paper – 21 Years On. *Applied Rheology*, 17(4):43110–1–43110–5, Aug. 2007. ISSN 1617-8106. doi: 10.1515/arh-2007-0012.

H. A. Barnes and J. F. Hutton. *An Introduction to Rheology*, volume 3. Elsevier, 1989.

R. Besseling, L. Isa, P. Ballesta, G. Petekidis, M. E. Cates, and W. C. K. Poon. Shear banding and flow-concentration coupling in colloidal glasses. *Physical Review Letters*, 105(26), Dec. 2010. ISSN 0031-9007, 1079-7114. doi: 10.1103/PhysRevLett.105.268301.

J. Bhatty and P. Banfill. Sedimentation behaviour in cement pastes subjected to continuous shear in rotational viscometers. *Cement and Concrete Research*, 12(1):69–78, Jan. 1982. ISSN 00088846. doi: 10.1016/0008-8846(82)90100-4.

B. Birkhofer. Doppler Ultrasound-Based Rheology. In I. T. Norton, F. Spyropoulos, and P. Cox, editors, *Practical Food Rheology: An Interpretive Approach*, Food Science and Technology. Wiley-Blackwell, Chichester, West Sussex ; Ames, Iowa, 2011. ISBN 978-1-4051-9978-0.

G. R. Bonin, V. T. Rombough, T. G. Carter, and M. G. Jefferies. Towards Better Injection Control and Verification of Rock Grouting. In *Grouting and Deep Mixing 2012*, pages 1460–1471, New Orleans, Louisiana, United States, Aug. 2012. American Society of Civil Engineers. ISBN 978-0-7844-1235-0. doi: 10.1061/9780784412350.0122.

D. Bonn, M. M. Denn, L. Berthier, T. Divoux, and S. Manneville. Yield Stress Materials in Soft Condensed Matter. *Reviews of Modern Physics*, 89(3), Aug. 2017. ISSN 0034-6861, 1539-0756. doi: 10.1103/RevModPhys.89.035005.

T. G. Carter, W. S. Dershowitz, D. Shuttle, and M. G. Jefferies. ACG_CArter_2012.pdf. In *Grouting and Deep Mixing 2012*, 2012.

T. G. Carter, M. G. Jefferies, V. T. Rombough, and W. S. Dershowitz. Aperture controlled grouting – benefits of the discrete fracture network approach. *Mining Technology*, 124(3):188–202, July 2015. ISSN 1474-9009, 1743-2863. doi: 10.1179/1743286315Y.0000000016.

Cementa. Cementa injektering 30 technical data sheet. `https://www.cementa.se/en/system/files_force/assets/document/injektering30eng.pdf?download=1`, 2013.

R. Chhabra and J. Richardson. *Non-Newtonian Flow and Applied Rheology*. Butterworth-Heinemann, Oxford, UK, second edition, July 2008. ISBN 978-0-7506-8532-0.

M. Christel, R. Yahya, M. Albert, and B. A. Antoine. Stick-slip control of the Carbopol microgels on polymethyl methacrylate transparent smooth walls. *Soft Matter*, 8(28):7365, 2012. ISSN 1744-683X, 1744-6848. doi: 10.1039/c2sm26244d.

CollyflowTech. Revolution pump specifications. `https://www.collyflowtech.se/Produkter/Pumpar/Kolvrotorpumpar/REVOLUTION/`, 2018.

P. Coussot. Experimental Procedures and Problems in Paste Viscometry. In *Rheometry of Pastes, Suspensions, and Granular Materials*, pages 81–152. John Wiley & Sons, Inc., Hoboken, NJ, USA, Jan. 2005. ISBN 978-0-471-72057-7 978-0-471-65369-1. doi: 10.1002/0471720577.ch3.

P. Coussot. *Rheophysics*. Soft and Biological Matter. Springer International Publishing, Cham, 2014a. ISBN 978-3-319-06147-4 978-3-319-06148-1. doi: 10.1007/978-3-319-06148-1.

P. Coussot. Yield stress fluid flows: A review of experimental data. *Journal of Non-Newtonian Fluid Mechanics*, 211:31–49, Sept. 2014b. ISSN 03770257. doi: 10.1016/j.jnnfm.2014.05.006.

P. Coussot, A. I. Leonov, and J. Piau. Rheology of concentrated dispersed systems in a low molecular weight matrix. *Journal of Non-Newtonian Fluid Mechanics*, 46:179–217, 1993.

P. Coussot, Q. D. Nguyen, H. T. Huynh, and D. Bonn. Avalanche Behavior in Yield Stress Fluids. *Physical Review Letters*, 88(17), Apr. 2002. ISSN 0031-9007, 1079-7114. doi: 10.1103/PhysRevLett.88.175501.

P. Coussot, H. Tabuteau, X. Chateau, L. Tocquer, and G. Ovarlez. Aging and solid or liquid behavior in pastes. *Journal of Rheology*, 50(6):975–994, Nov. 2006. ISSN 0148-6055, 1520-8516. doi: 10.1122/1.2337259.

G. Dai and R. Bird. Radial flow of a Bingham fluid between two fixed circular disks. *Journal of Non-Newtonian Fluid Mechanics*, 8(3-4):349–355, Jan. 1981. ISSN 03770257. doi: 10.1016/0377-0257(81)80031-6.

Y. Damianou and G. C. Georgiou. Viscoplastic Poiseuille flow in a rectangular duct with wall slip. *Journal of Non-Newtonian Fluid Mechanics*, 214: 88–105, Dec. 2014. ISSN 03770257. doi: 10.1016/j.jnnfm.2014.10.002.

Y. Damianou, G. Kaoullas, and G. C. Georgiou. Cessation of viscoplastic Poiseuille flow in a square duct with wall slip. *Journal of Non-Newtonian Fluid Mechanics*, 233:13–26, July 2016. ISSN 03770257. doi: 10.1016/j.jnnfm.2015.11.002.

E. Di Giuseppe, F. Corbi, F. Funiciello, A. Massmeyer, T. Santimano, M. Rosenau, and A. Davaille. Characterization of Carbopol® hydrogel rheology for experimental tectonics and geodynamics. *Tectonophysics*, 642:29–45, Feb. 2015. ISSN 00401951. doi: 10.1016/j.tecto.2014.12.005.

M. Dinkgreve, M. M. Denn, and D. Bonn. "Everything flows?": Elastic effects on startup flows of yield-stress fluids. *Rheologica Acta*, 56(3):189–194, Mar. 2017. ISSN 0035-4511, 1435-1528. doi: 10.1007/s00397-017-0998-z.

T. Divoux, D. Tamarii, C. Barentin, S. Teitel, and S. Manneville. Yielding dynamics of a Herschel–Bulkley fluid: A critical-like fluidization behaviour. *Soft Matter*, 8(15):4151, 2012. ISSN 1744-683X, 1744-6848. doi: 10.1039/c2sm06918k.

T. Divoux, M. A. Fardin, S. Manneville, and S. Lerouge. Shear Banding of Complex Fluids. *Annual Review of Fluid Mechanics*, 48 (1):81–103, Jan. 2016. ISSN 0066-4189, 1545-4479. doi: 10.1146/annurev-fluid-122414-034416.

N. Dogan, M. J. McCarthy, and R. L. Powell. In-Line Measurement of Rheological Parameters and Modeling of Apparent Wall Slip in Diced Tomato Suspensions Using Ultrasonics. *Food Engineering and Physical Properties*, 67(6):2235–2240, 2002.

D. Doraiswamy. The Origins of Rheology: A Short Historical Excursion. *Rheology Bulletin*, 71:9, 2002.

A. Draganović and H. Stille. Filtration of cement-based grouts measured using a long slot. *Tunnelling and Underground Space Technology*, 43: 101–112, July 2014. ISSN 08867798. doi: 10.1016/j.tust.2014.04.010.

M. El Tani. Grouting Rock Fractures with Cement Grout. *Rock Mechanics and Rock Engineering*, 45(4):547–561, July 2012. ISSN 0723-2632, 1434-453X. doi: 10.1007/s00603-012-0235-0.

M. El Tani. Grouting Emancipation. *GeoTech News*, 31(3):38–42, Sept. 2013.

K. Fernandez, B. Pyzdrowski, D. W. Schiller, and M. B. Smith. Understand the basics of centrifugal pump operation. *CEP Magazine, May*, 5256, 2002.

L. Ferrás, J. Nóbrega, and F. Pinho. Analytical solutions for Newtonian and inelastic non-Newtonian flows with wall slip. *Journal of Non-Newtonian Fluid Mechanics*, 175-176:76–88, May 2012. ISSN 03770257. doi: 10.1016/j.jnnfm.2012.03.004.

R. D. Ferron, S. Shah, E. Fuente, and C. Negro. Aggregation and breakage kinetics of fresh cement paste. *Cement and Concrete Research*, 50:1–10, Aug. 2013. ISSN 00088846. doi: 10.1016/j.cemconres.2013.03.002.

Å. Fransson, J. Funehag, and J. Thörn. Swedish grouting design: Hydraulic testing and grout selection. *Proceedings of the Institution of Civil Engineers - Ground Improvement*, 169(4):275–285, Nov. 2016. ISSN 1755-0750, 1755-0769. doi: 10.1680/jgrim.15.00020.

I. Frigaard. Simple yield stress fluids. *Current Opinion in Colloid & Interface Science*, 43:80–93, Oct. 2019. ISSN 13590294. doi: 10.1016/j.cocis.2019.03.002.

J. Funehag. *Grouting of Fractured Rock with Silica Sol*. PhD thesis, Chalmers University of Technology, Göteborg, Sweden, 2007.

J. Funehag and J. Thörn. Radial penetration of cementitious grout – Laboratory verification of grout spread in a fracture model. *Tunnelling and Underground Space Technology*, 72:228–232, Feb. 2018. ISSN 08867798. doi: 10.1016/j.tust.2017.11.020.

S. A. Greenberg and L. M. Meyer. Rheology of Fresh Portland Cement Pastes-Influence of Calcium Sulfates. *Highway Research Record*, page 21, 1963.

J. Guo, H. Shan, Z. Xie, C. Li, H. Xu, and Z. Jianmin. Exact Solution to Navier-Stokes Equation for Developed Radial Flow between Parallel Disks. *Journal of Engineering Mechanics*, 143(6):10, 2017.

G. Gustafson and H. Stille. Stop criteria for cement grouting. *Felsbau*, 23 (3):62–68, 2005.

G. Gustafson, J. Claesson, and Å. Fransson. Steering Parameters for Rock Grouting. *Journal of Applied Mathematics*, 2013, 2013.

U. Håkansson. *Rheology of Fresh Cement-Based Grouts*. PhD dissertation, Royal Institute of Technology, Stockholm, 1993.

U. Håkansson, L. Hässler, and H. Stille. Rheological properties of microfine cement grouts. *Tunnelling and Underground Space Technology*, 7(4): 453–458, 1992.

U. Håkansson, J. Wiklund, and M. Kotzé. In-Line Determination of Cement-Based Grout Properties Using a Pulsed Ultrasound Based Method and System. In *Grouting 2017*, pages 356–367, Honolulu, Hawaii, July 2017. American Society of Civil Engineers. ISBN 978-0-7844-8079-3. doi: 10.1061/9780784480793.034.

L. Hässler. *Grouting of Rock - Simulation and Classification*. PhD dissertation, Royal Institute of Technology (KTH), Stockholm, 1991.

V. T. Hoang, W. Liu, and J. M. Park. Discussion on "Analysis of Bingham fluid radial flow in smooth fractures" [J Rock Mech Geotech Eng 12 (2020) 1112–1118]. *Journal of Rock Mechanics and Geotechnical Engineering*, page S1674775521000408, Mar. 2021. ISSN 16747755. doi: 10.1016/j.jrmge.2021.03.001.

A. C. Houlsby. *Construction and Design of Cement Grouting: A Guide to Grouting in Rock Foundations*. Wiley-Interscience, 1st edition, May 1990. ISBN 978-0-471-51629-3.

ISEL. Isel LEZ1 belt-actuator technical specifications. `https://www.isel-us.com/LEZ-1-Belt-Actuator`, 2021.

S. Jarny, N. Roussel, S. Rodts, F. Bertrand, R. Le Roy, and P. Coussot. Rheological behavior of cement pastes from MRI velocimetry. *Cement and Concrete Research*, 35(10):1873–1881, Oct. 2005. ISSN 00088846. doi: 10.1016/j.cemconres.2005.03.009.

S. Jarny, N. Roussel, R. Le Roy, and P. Coussot. Modelling thixotropic behavior of fresh cement pastes from MRI measurements. *Cement and Concrete Research*, 38(5):616–623, May 2008. ISSN 00088846. doi: 10.1016/j.cemconres.2008.01.001.

J. A. Jensen. *Estimation Of Blood Velocities Using Ultrasound: A Signal Processing Approach*. Cambridge University Press, 1996.

D. M. Kalyon. Apparent slip and viscoplasticity of concentrated suspensions. *Journal of Rheology*, 49(3):621–640, May 2005. ISSN 0148-6055, 1520-8516. doi: 10.1122/1.1879043.

V. Kelessidis, R. Maglione, C. Tsamantaki, and Y. Aspirtakis. Optimal determination of rheological parameters for Herschel–Bulkley drilling fluids and impact on pressure drop, velocity profiles and penetration rates during drilling. *Journal of Petroleum Science and Engineering*, 53(3-4):203–224, Sept. 2006. ISSN 09204105. doi: 10.1016/j.petrol.2006.06.004.

H.-M. Kim, J.-W. Lee, M. Yazdani, E. Tohidi, H. R. Nejati, and E.-S. Park. Coupled Viscous Fluid Flow and Joint Deformation Analysis for Grout Injection in a Rock Joint. *Rock Mechanics and Rock Engineering*, 51(2):627–638, Feb. 2018. ISSN 0723-2632, 1434-453X. doi: 10.1007/s00603-017-1339-3.

S. K. Kim. Flow rate based framework for solving viscoplastic flow with slip. *Journal of Non-Newtonian Fluid Mechanics*, 269:37–46, July 2019. ISSN 03770257. doi: 10.1016/j.jnnfm.2019.06.002.

S. Kobayashi, H. Stille, G. Gustafson, and B. Stille. Real Time Grouting Control Method - Development and application using - Äspö HRL data. Technical Report R-08-133, Swedish Nuclear Fuel and Waste Management Company, Stockholm, 2008.

Krohne. Electromagnetic flow sensor specifications: Optiflux 4000. `https://krohne.com/en/products/flow-measurement/components-and-peripheral-equipment-for-flow-measurement/flow-sensors/optiflux-4000/`, 2021.

B. R. Laurencena and M. C. Williams. Radial Flow of Non-Newtonian Fluids Between Parallel Plates. *Transactions of the Society of Rheology*, 18(3):331–355, Sept. 1974. ISSN 0038-0032. doi: 10.1122/1.549339.

G. Lipscomb and M. Denn. Flow of bingham fluids in complex geometries. *Journal of Non-Newtonian Fluid Mechanics*, 14:337–346, Jan. 1984. ISSN 03770257. doi: 10.1016/0377-0257(84)80052-X.

G. Lombardi. The role of cohesion in cement grouting of rock. In *International Commission on Large Dams*, Lausanne, 1985.

G. Lombardi. Selecting the grouting intensity. *The International Journal on Hydropower and Dams*, (4):62–66, 1996.

G. Lombardi. GIN again misunderstood. *GeoTech News*, 25(2):35–37, 2007.

G. Lombardi. Misunderstanding of GIN confirmed. *GeoTech News*, 26(2): 57–63, 2008.

G. Lombardi and D. Deere. Grouting design and control using the GIN principle. *International Water Power and Dam Construction*, 46:15–22, June 1993.

C. Louis. *A Study of Ground Water Flow in Jointed Rock and Its Influence on the Stability of Rock Masses*. 10. London, Eng. : Imperial College of Science and Technology, 1969.

Lubrizol. Neutralizing Carbopol® and Pemulen™ Polymers in Aqueous and Hydroalcoholic Systems, Sept. 2009.

Lubrizol. Neutralization Procedures, May 2011.

R. Majidi, S. Z. Miska, R. Ahmed, M. Yu, and L. G. Thompson. Radial flow of yield-power-law fluids: Numerical analysis, experimental study and the application for drilling fluid losses in fractured formations. *Journal of Petroleum Science and Engineering*, 70(3-4):334–343, Feb. 2010. ISSN 09204105. doi: 10.1016/j.petrol.2009.12.005.

M. H. Mohammed, R. Pusch, and S. Knutsson. Study of cement-grout penetration into fractures under static and oscillatory conditions. *Tunnelling and Underground Space Technology*, 45:10–19, Jan. 2015. ISSN 08867798. doi: 10.1016/j.tust.2014.08.003.

P. Moller, A. Fall, V. Chikkadi, D. Derks, and D. Bonn. An attempt to categorize yield stress fluid behaviour. *Philosophical Transactions of the Royal Society A: Mathematical, Physical and Engineering Sciences*, 367 (1909):5139–5155, Dec. 2009. ISSN 1364-503X, 1471-2962. doi: 10.1098/rsta.2009.0194.

P. C. F. Møller, J. Mewis, and D. Bonn. Yield stress and thixotropy: On the difficulty of measuring yield stresses in practice. *Soft Matter*, 2(4):274, 2006. ISSN 1744-683X, 1744-6848. doi: 10.1039/b517840a.

P. C. F. Møller, S. Rodts, M. A. J. Michels, and D. Bonn. Shear banding and yield stress in soft glassy materials. *Physical Review E*, 77(4), Apr. 2008. ISSN 1539-3755, 1550-2376. doi: 10.1103/PhysRevE.77.041507.

L. Muravleva. Axisymmetric squeeze flow of a viscoplastic Bingham medium. *Journal of Non-Newtonian Fluid Mechanics*, 249:97–120, Nov. 2017. ISSN 03770257. doi: 10.1016/j.jnnfm.2017.09.006.

T. Y. Na and A. G. Hansen. Radial flow of viscous non-Newtonian fluids between disks. *International Journal of Non-Linear Mechanics*, 2(3): 261–273, Sept. 1967. ISSN 00207462. doi: 10.1016/0020-7462(67)90027-3.

A. Nejad Ghafar. *An Experimental Study to Measure Grout Penetrability, Improve the Grout Spread, and Evaluate the Real Time Grouting Control Theory.* Dissertation, KTH Royal Institute of Technology, Stockholm, 2017.

Q. D. Nguyen and D. V. Boger. Measuring the Flow Properties of Yield Stress Fluids. *Annual Review of Fluid Mechanics*, 24(1):47–88, 1992. doi: 10.1146/annurev.fl.24.010192.000403.

P. D. Olmsted. Perspectives on shear banding in complex fluids. *Rheologica Acta*, 47(3):283–300, Apr. 2008. ISSN 0035-4511, 1435-1528. doi: 10.1007/s00397-008-0260-9.

G. Ovarlez. Introduction to the rheometry of complex suspensions. In *Understanding the Rheology of Concrete*, pages 23–62. Elsevier, 2012. ISBN 978-0-85709-028-7. doi: 10.1533/9780857095282.1.23.

G. Ovarlez and S. Hormozi. *Visco-Plastic Fluids: From Theory to Application.* Springer Berlin Heidelberg, New York, NY, 2018. ISBN 978-3-319-89437-9.

G. Ovarlez, S. Rodts, X. Chateau, and P. Coussot. Phenomenology and physical origin of shear localization and shear banding in complex fluids. *Rheologica Acta*, 48(8):831–844, Oct. 2009. ISSN 0035-4511, 1435-1528. doi: 10.1007/s00397-008-0344-6.

G. Ovarlez, F. Mahaut, F. Bertrand, and X. Chateau. Flows and heterogeneities with a vane tool: Magnetic resonance imaging measurements. *Journal of Rheology*, 55(2):197–223, Mar. 2011. ISSN 0148-6055, 1520-8516. doi: 10.1122/1.3526349.

G. Ovarlez, F. Bertrand, P. Coussot, and X. Chateau. Shear-induced sedimentation in yield stress fluids. *Journal of Non-Newtonian Fluid Mechanics*, 177-178:19–28, June 2012. ISSN 03770257. doi: 10.1016/j.jnnfm.2012.03.013.

J. M. Park. Flow classification of radial and squeeze flows between parallel disks. *Journal of Non-Newtonian Fluid Mechanics*, 286:104416, Dec. 2020. ISSN 03770257. doi: 10.1016/j.jnnfm.2020.104416.

F. Pignon, A. Magnin, and J.-M. Piau. Thixotropic colloidal suspensions and flow curves with minimum: Identification of flow regimes and rheometric consequences. *Journal of Rheology*, 40(4):573–587, July 1996. ISSN 0148-6055, 1520-8516. doi: 10.1122/1.550759.

R. L. Powell. Experimental techniques for multiphase flows. *Physics of Fluids*, 20(4):040605, 2008. ISSN 10706631. doi: 10.1063/1.2911023.

A. M. V. Putz and T. I. Burghelea. The solid–fluid transition in a yield stress shear thinning physical gel. *Rheologica Acta*, 48(6):673–689, July 2009. ISSN 0035-4511, 1435-1528. doi: 10.1007/s00397-009-0365-9.

Y. Qian and S. Kawashima. Distinguishing dynamic and static yield stress of fresh cement mortars through thixotropy. *Cement and Concrete Composites*, 86:288–296, Feb. 2018. ISSN 09589465. doi: 10.1016/j.cemconcomp.2017.11.019.

M. Rahman, U. Håkansson, and J. Wiklund. In-line rheological measurements of cement grouts: Effects of water/cement ratio and hydration. *Tunnelling and Underground Space Technology*, 45:34–42, Jan. 2015. ISSN 08867798. doi: 10.1016/j.tust.2014.09.003.

M. Rahman, J. Wiklund, R. Kotzé, and U. Håkansson. Yield stress of cement grouts. *Tunnelling and Underground Space Technology*, 61:50–60, Jan. 2017. ISSN 08867798. doi: 10.1016/j.tust.2016.09.009.

V. Rombough, D. Bonn, and D. Shuttle. Penetrability control of the GIN mixes during fractured rock grouting. In *Proceedings of the 59th Canadian Geotechnical Conference*, pages 528–535, Vancouver, BC, Canada, Oct. 2006.

N. Roussel. Steady and transient flow behaviour of fresh cement pastes. *Cement and Concrete Research*, 35(9):1656–1664, Sept. 2005. ISSN 00088846. doi: 10.1016/j.cemconres.2004.08.001.

N. Roussel. *Understanding the Rheology of Concrete*. Woodhead Publishing Series in Civil and Structural Engineering. Elsevier Science & Technology, 2016. ISBN 978-0-08-101645-9.

F. J. Rubio-Hernández, N. M. Páez-Flor, and J. F. Velázquez-Navarro. Why monotonous and non-monotonous steady-flow curves can be obtained with the same non-Newtonian fluid? A single explanation. *Rheologica Acta*, 57(5):389–396, May 2018. ISSN 0035-4511, 1435-1528. doi: 10.1007/s00397-018-1084-x.

S. Satomura. Ultrasonic Doppler Method for the Inspection of Cardiac Functions. *The Journal of the Acoustical Society of America*, 29(11): 1181–1185, 1957.

S. B. Savage. Laminar Radial Flow Between Parallel Plates. *Journal of Applied Mechanics*, 31(4):594, 1964. ISSN 00218936. doi: 10.1115/1.3629719.

T. J. Shamu and U. Håkansson. Rheology of cement grouts: On the critical shear rate and no-slip regime in the Couette geometry. *Cement and Concrete Research*, page S0008884619301437, May 2019. ISSN 00088846. doi: 10.1016/j.cemconres.2019.05.014.

T. J. Shamu, R. Kotze, and J. Wiklund. Acoustic characterization of pulsed ultrasound sensors for improved non-invasive Pulsed Ultrasound Velocimetry through high-grade stainless steel pipes. In *10th International Symposium on Ultrasonic Doppler Methods for Fluid Mechanics and Fluid Engineering*, Tokyo, Japan, Sept. 2016. ISUD.

T. J. Shamu, L. Zou, R. Kotzé, J. Wiklund, and U. Håkansson. Radial flow velocity profiles of a yield stress fluid between smooth parallel disks. *Rheologica Acta*, 59(4):239–254, 2020. doi: 10.1007/s00397-020-01203-x.

T. J. Shamu, L. Zou, and U. Håkansson. An experimental device for measuring radial flow velocity profiles of yield stress fluids. *Submitted to Flow Measurement and Instrumentation*, Aug. 2021a.

T. J. Shamu, L. Zou, and U. Håkansson. A nomogram for cement-based rock grouting. *Tunnelling and Underground Space Technology*, 116:104110, Oct. 2021b. ISSN 08867798. doi: 10.1016/j.tust.2021.104110.

R. Shaughnessy and P. E. Clark. The rheological behavior of fresh cement pastes. *Cement and Concrete Research*, 18(3):327–341, May 1988. ISSN 00088846. doi: 10.1016/0008-8846(88)90067-1.

D. Shuttle, V. Rombough, and G. Bonin. Impact of Grout Rheology on GIN. In *Grouting for Ground Improvement*, pages 1–10, Denver, Colorado, United States, Oct. 2007a. American Society of Civil Engineers. ISBN 978-0-7844-0912-1. doi: 10.1061/40912(231)3.

D. Shuttle, V. T. Rombough, and G. R. Bonin. GIN Distilled. *GeoTech News*, 31(2):24–25, Sept. 2007b.

D. Shuttle, V. T. Rombough, and G. R. Bonin. An alternative viewpoint on GIN. *GeoTech News*, 26(2):64–66, 2008.

T. Sochi. Slip at Fluid-Solid Interface. *arXiv:1101.4421 [physics]*, Jan. 2011. doi: 10.1080/15583724.2011.615961.

H. Stille. *Rock Grouting - Theories and Applications*. Vulkanmedia, Stockholm, Sept. 2015.

TA-Instruments. AR-2000ex rheometer brochure and specifications. `http://www.tainstruments.com/pdf/brochure/2006_AR_Brochure.pdf`, 2006.

Y. Takeda. Development of an ultrasound velocity profile monitor. *Nuclear Engineering and Design*, 126:277–284, 1991.

Y. Takeda. *Ultrasonic Doppler Velocity Profiler for Fluid Flow*, volume 101. Springer, Tokyo, Japan, 2012.

U. S. Army Corps of Engineers. Engineering and Design Grouting Technology, Mar. 2017.

J. Van Wazer, R. ColWell, K. Kim, and J. Lyons. *Viscosity and Flow Measurement. A Laboratory Handbook of Rheology. By J.R. van Wazer, J.W. Lyons, K.Y. Kim, and R.E. Colwell. [With Illustrations.].* New York, London, 1963.

O. H. Wallevik and J. E. Wallevik. Rheology as a tool in concrete science: The use of rheographs and workability boxes. *Cement and Concrete Research*, 41(12):1279–1288, Dec. 2011. ISSN 00088846. doi: 10.1016/j.cemconres.2011.01.009.

M. Wallner. *Propagation of Sedimentation Stable Cement Pastes in Jointed Rock*. PhD thesis, University of Aachen, BRD, Inst Found Engng, Soil Mech, Rock Mech, Waterways Constr, 1976.

J. Wiklund and M. Stading. Application of in-line ultrasound Doppler-based UVP–PD rheometry method to concentrated model and industrial suspensions. *Flow Measurement and Instrumentation*, 19(3-4):171–179, June 2008. ISSN 09555986. doi: 10.1016/j.flowmeasinst.2007.11.002.

A. Yahia and K. Khayat. Analytical models for estimating yield stress of high-performance pseudoplastic grout. *Cement and Concrete Research*, 31(5): 731–738, May 2001. ISSN 00088846. doi: 10.1016/S0008-8846(01)00476-8.

M. Yamamoto, J. Carrillo, A. Insunza, G. Mari, and Y. Ville. Error introduced into velocity measurements by inappropriate Doppler angle assignment. *Ultrasound in Obstetrics & Gynecology*, 28(6):853–854, 2006.

Y. L. Yeow and J. W. Taylor. Obtaining the shear rate profile of steady laminar tube flow of Newtonian and non-Newtonian fluids from nuclear magnetic resonance imaging and laser Doppler velocimetry data. *Journal of Rheology*, 46(2):351–365, Mar. 2002. ISSN 0148-6055, 1520-8516. doi: 10.1122/1.1446881.

E. Younes, V. Bertola, C. Castelain, and T. Burghelea. Slippery flows of a Carbopol gel in a microchannel. *Physical Review Fluids*, 5(8):083303, Aug. 2020. ISSN 2469-990X. doi: 10.1103/PhysRevFluids.5.083303.

L. Zou, U. Håkansson, and V. Cvetkovic. Two-phase cement grout propagation in homogeneous water-saturated rock fractures. *International Journal of Rock Mechanics and Mining Sciences*, 106:243–249, June 2018. ISSN 13651609. doi: 10.1016/j.ijrmms.2018.04.017.

L. Zou, U. Håkansson, and V. Cvetkovic. Analysis of Bingham fluid radial flow in smooth fractures. *Journal of Rock Mechanics and Geotechnical Engineering*, 12(5):1112–1118, Oct. 2020a. ISSN 16747755. doi: 10.1016/j.jrmge.2019.12.021.

L. Zou, U. Håkansson, and V. Cvetkovic. Radial propagation of yield-power-law grouts into water-saturated homogeneous fractures. *International Journal of Rock Mechanics and Mining Sciences*, 130:104308, June 2020b. ISSN 13651609. doi: 10.1016/j.ijrmms.2020.104308.

L. Zou, U. Håkansson, and V. Cvetkovic. Reply to Discussion on "Analysis of Bingham fluid radial flow in smooth fractures". *Journal of Rock Mechanics and Geotechnical Engineering*, page S1674775521000512, May 2021. ISSN 16747755. doi: 10.1016/j.jrmge.2021.04.001.

Appended papers